Science of the Total Environment 778 (2021) 146017

Contents lists available at ScienceDirect

Science of the Total Environment

journal homepage: www.elsevier.com/locate/scitotenv

Climate and land cover change impacts on stormwater runoff in large-scale coastal-urban environments

Erfanul Huq, Omar I. Abdul-Aziz *

Department of Civil and Environmental Engineering, West Virginia University, 395 Evansdale Drive, Morgantown, WV 26506-6103, USA

HIGHLIGHTS

- A large-scale stormwater model was developed with EPA SWMM for southeast Florida.
- The coastal-urban environments had a predominant climatic control on runoff changes.
- Concurrent climatic and land cover changes led to synergistic changes in runoff.
- High increases (80–118%) in coastal-urban runoff were projected by 2050s and 2080s.
- Higher increases in runoff and flooding risk were noted in the urban centers.

GRAPHICAL ABSTRACT

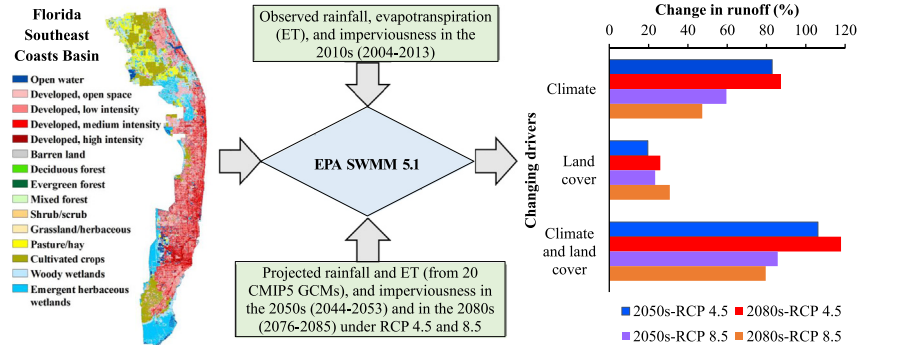

ARTICLE INFO

Article history:
Received 28 October 2020
Received in revised form 6 February 2021
Accepted 16 February 2021
Available online 23 February 2021

Editor: Fernando A.L. Pacheco

Keywords:
Climatic and land cover changes
Coastal-urban centers
Mechanistic modeling
Southeast Florida
Stormwater runoff sensitivity and future scenarios
SWMM

ABSTRACT

This study aims to evaluate the individual and synergistic controls of climatic and land cover changes on stormwater runoff regimes, and perform a comparative synthesis of the historical and future runoffs for complex coastal-urban environments. A large-scale (7117 km^2) mechanistic hydrologic model was developed for Florida Southeast Coasts Basin as the study area using U.S. Environmental Protection Agency (EPA)'s Storm Water Management Model 5.1. The model was calibrated and validated with daily streamflow observations (Nash-Sutcliffe Efficiency = 0.74 to 0.92) during 2004–2013 (termed 2010s), computing the corresponding runoff volume as a historical reference. Runoffs for 2050s (2044–2053) and 2080s (2076–2085) were quantified by incorporating climatic projections from 20 General Circulation Models and land cover projections from EPA under the Representative Concentration Pathways (RCP) 4.5 and 8.5 scenarios. We found a predominant climatic control on the potential runoff changes and a high vulnerability in the coastal-urban environments. The concurrent changes in climate and land cover led to synergistic (stronger than the sum of individual effects) nonlinear responses of runoff. The projected changes in climate and land cover together would increase the annual basin runoff volume by 118%, 106%, 86%, and 80% under the 2080s-RCP 4.5, 2050s-RCP 4.5, 2050s-RCP 8.5, and 2080s-RCP 8.5 scenarios, respectively. Greater increases in runoff were noted at and around the urban centers than that at the non-urban areas across the basin. The relative increases in runoff were higher during the dry season and transitional months (October–May) than the wet season (June–September). Our findings would guide stormwater management and ecosystem protection for southeast Florida and coastal built environments across the world.

1. Introduction

The increasing global temperature is expected to increase rainfall and stormwater runoff in high latitude and wet tropical areas; however,

* Corresponding author.
E-mail address: oiabdulaziz@mail.wvu.edu (O.I. Abdul-Aziz).

https://doi.org/10.1016/j.scitotenv.2021.146017
0048-9697/

dry tropical and semi-arid regions are expected to experience decrease in rainfall and runoff (IPCC, 2014a). Human interventions can also impact watershed runoff and streamflow generation processes (e.g., Miller et al., 2014; Diem et al., 2018; Li et al., 2018). Reduced soil infiltration capacity from increased impervious cover together with diminished depressional storage can lead to an increase in speed and volume of runoff generation. Increased drainage density (i.e., total length of drainage channel per unit area of the drainage basin) can contribute to faster and higher peaks of flow rate in the receiving streams. A changing climate and hydrology, in concert with increasing urbanization and built environments, would substantially affect the urban hydrologic processes (Pumo et al., 2017; Wang et al., 2020). Urbanization and climate change can specifically increase widespread flooding risks in cities, amounting to an annual estimated loss of $52 billion globally by the mid-21st century (Hallegatte et al., 2013). A comprehensive analysis and understanding of potential changes in urban runoff regimes is, therefore, necessary to adjust for the detrimental outcomes under future developments and climatic changes (Jacobson, 2011).

Much research has been conducted to investigate the influence of various environmental drivers on stormwater runoff and receiving streamflow in watersheds around the world. In particular, runoff sensitivity to the historical and/or experimental changes in climate and land cover has been a major research focus for decades (e.g., Abdul-Aziz and Al-Amin, 2015; Mateus et al., 2015; Hasan et al., 2018; Bharat and Mishra, 2020). Mechanistic (process-based) models have been used by ample studies for simulation of both hydrologic (e.g., Fukunaga et al., 2015; Rai et al., 2017; Ul Islam et al., 2019; Hu and Shrestha, 2020) and hydrodynamic (e.g., Ghani et al., 2010; Julien et al., 2010; Liu et al., 2015; Zainalfikry et al., 2020) responses in watersheds and receiving streams. For runoff sensitivity analyses, mechanistic hydrologic models have been extensively employed by conceptualizing and parameterizing various environmental drivers and watershed components of stormwater runoff and streamflow. For example, Wang et al. (2017) employed the SWBM model (Zhang and Wang, 2007) to compute runoff sensitivities to climatic changes in 21 climatically different catchments across China. The authors reported notable decreases in runoff under a 10% precipitation decrease scenario. Olang and Fürst (2011) found notable increases in annual runoff due to land cover changes between 1973 and 2002 by using the HEC-HMS model (USACE, 2000) for the Nyando River Basin in Kenya. Cuo et al. (2013) employed the Variable Infiltration Capacity (VIC; Liang et al., 1994) model in the Yellow River Basin of China. They reported significant changes in seasonal and annual streamflow due to changes in precipitation, evapotranspiration (ET), and land cover during 1957–2009.

Mechanistic hydrologic models have also been widely used to compute potential changes in watershed runoff and streamflow by incorporating the projected future changes in climate and land cover. Zheng et al. (2018) used a global hydrological model, H08 (Hanasaki et al., 2008a, 2008b) to report increases in mean annual runoff from the projected climatic changes during 2046–2075, relative to the 1976–2005 baseline, across the Indian subcontinent of south Asia. Franczyk and Chang (2009) employed Soil and Water Assessment Tool (SWAT; Neitsch et al., 2005), and reported potential increases in annual runoff due to the projected increases in precipitation and urbanization during 2030–2059 (relative to 1973–2002) for the Rock Creek Basin in Portland, Oregon, USA. Wagesho et al. (2012) built a model with SWAT for the Rift Valley Lakes Basin of Ethiopia, and found both increases and decreases in annual runoff across the basin under the projected climate during 2080–89, relative to 1990–99. Oo et al. (2020) reported potential decreases in streamflow due to the projected climatic changes during 2020–2100, relative to 1991–2015, by developing a SWAT model for the Upper Ayeyarwady River Basin in Myanmar. Al-Safi et al. (2020) employed a physically based distributed model, BTOPMC (Al-Safi and Sarukkalige, 2019) and found notable changes in runoff from climatic changes during 2046–2065 and 2080–2099 (relative to 1982–2014) for different basins in Australia.

Although the existing literature on the effects of changing climate and land cover on runoff has represented different regions of the world, research focusing on the thriving coastal-urban environments has been scarce. Further investigation is, therefore, warranted to assess vulnerabilities and achieve resilience in coastal-urban environments, which often accommodate major population centers and economic hubs. Southeast Florida of USA is an ideal representation of complex coastal-urban hydrologic settings with a highly complex drainage network and continuing developments since the 20th century (Hughes and White, 2016). One of the few hydrologic modeling studies in this area was conducted by Abdul-Aziz and Al-Amin (2015); they quantified the individual as well as combined hydro-climatic and land cover sensitivities of stormwater runoff in the Miami River Basin (drainage area ~175 km^2) of Florida. The study reported rainfall as the stronger controlling driver of runoff than land cover, with salient seasonal variation. They also reported a stronger, nonlinear response of runoff to concurrent changes in climate (rainfall) and land cover (imperviousness) than the linear summation of their standalone, individual effects. The study, however, encompassed a relatively small area of southeast Florida and did not incorporate future projections of climate or land cover to evaluate the potential impacts on stormwater runoff. Obeysekera et al. (2015) examined the hydrologic responses in south Florida by adopting a climate sensitivity approach. Their findings indicated potentially significant changes in the regional water budgets, ecosystem performance, and in water supply demands for the near future. However, the authors also did not explicitly incorporate projected climatic and land cover changes to determine the potential impacts on runoff in their study.

This paper aims to determine the controls of climatic and land cover drivers on stormwater runoff, and perform a comparative synthesis of historical and projected future runoff scenarios for large-scale complex coastal-urban environments. The underlying research hypothesis is that climatic and land cover changes would overall substantially increase stormwater runoff in tropical/sub-tropical coastal-urban environments. We focus on the pluvial runoff volume (excess rainfall on the ground) as the stormwater runoff based on conventional terminologies (Falconer et al., 2009; Carter et al., 2015; Rosenzweig et al., 2018). A large-scale mechanistic hydrologic model is developed for the Southeast Coasts Basin of Florida as the study area by using the Storm Water Management Model (SWMM) 5.1 of U.S. Environmental Protection Agency (U.S. EPA; Rossman, 2015). The model is calibrated and validated with historical streamflows. Stormwater runoff sensitivities to reference changes in climatic variables and land cover features are first computed. The future stormwater runoff for the basin is then computed by inputting projections of climatic and land cover variables into the model — identifying areas with potential risks of exacerbated flooding and environmental pollutions.

2. Materials and methods

2.1. Study area

The Florida Southeast Coasts Basin drains an area of approximately 7117 km^2 (Fig. 1). Majority of the basin represents highly urbanized land uses such as single-family housing units, apartment complexes, and commercial and industrial areas. However, the western (especially northwestern) and southern parts of the basin represent significant other land uses, including croplands, pasture lands, and wetlands (Fig. 1). Miami, Fort Lauderdale, West Palm Beach, Doral, Hialeah, Delray Beach, Boca Raton, and Hollywood are the eminent, highly urbanized, and evergrowing cities in the basin. Further, the cities of Homestead, Weston, Sunrise, Jupiter, Fort Pierce, and Port St. Lucie represent other fast growing urban centers in this coastal-urban basin.

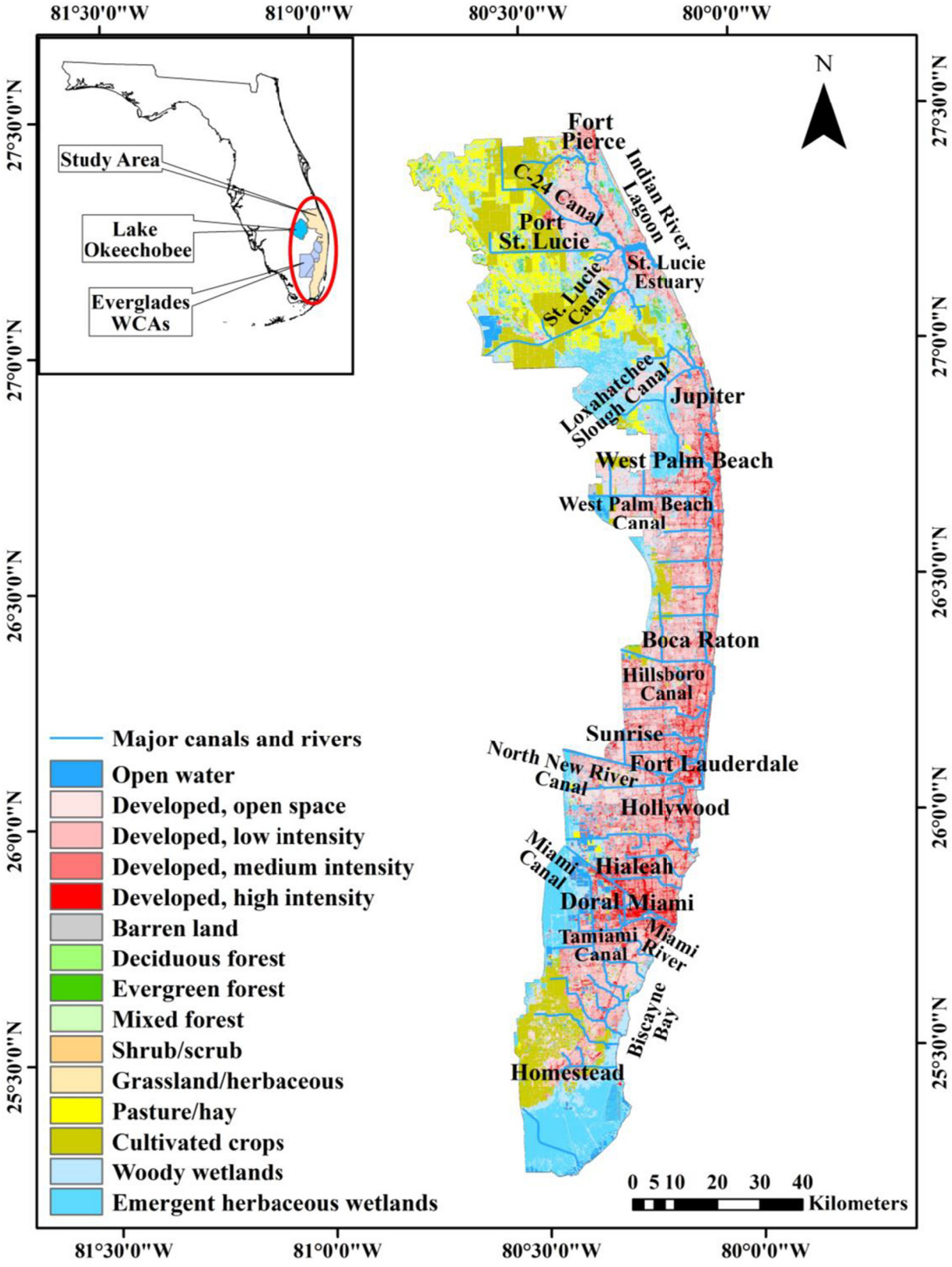

Fig. 1. Major canals, rivers, and land cover types in the Southeast Coasts Basin. Inset shows the locations of the study area, Lake Okeechobee, and the Everglades Water Conservation Areas (WCAs) in the state of Florida. Inset is not drawn to the map-scale.

A distinct and complex drainage networks of rivers and canals drain the Southeast Coasts Basin to the Atlantic Ocean (Fig. 1; Fig. S1 in Supplementary materials). Tamiami Canal (also known as C4 canal), Miami River (C6 canal), North New River Canal, Hillsboro Canal, West Palm Beach Canal, St. Lucie River, and Loxahatchee Slough Canal are some of the major streams in the basin. Most major streams originate from Lake Okeechobee (the largest freshwater lake in Florida), and pass through the Everglades Water Conservation Areas (WCAs) before

entering the Southeast Coasts Basin. These streams typically drain into the estuarine water bodies (e.g., St. Lucie Estuary, Indian River Lagoon, and Biscayne Bay), prior to reaching the Atlantic Ocean. The rivers and canals are managed by control structures and gates to mitigate flooding and salinity intrusion.

As per the Köppen-Geiger climate classification (Kottek et al., 2006; Rubel et al., 2017), there is a gradient of climate zones across the study basin (ORNL, 2017). The upper northeastern part (e.g., Port St. Lucie) is characterized by humid subtropical climate with highly varying rainfall over the year. However, places such as Jupiter experience tropical rainforest climate with approximately uniformly distributed rainfall over the year. The middle part of the basin from Miami to West Palm Beach is predominantly subject to tropical climate with a relatively long monsoon season and a short dry season. The lower southern part (e.g., Homestead) undergoes tropical savannah climate having longer dry seasons than tropical monsoon climate. On basin-scale average, the Southeast Coasts Basin received mean annual rainfall of 1583 mm (NOAA, 2021) during 1981–2010. In contrast, the mean annual temperature during 1981–2010 ranged from 68 to 83 °F, with an average temperature of 75 °F. For majority of the basin, land surface elevation varies from 0.01 to 7.5 m, with respect to the North American Vertical Datum of 1988 (NAVD 88; Fig. S2 in Supplementary materials). The basin also represented various hydrologic soil groups (e.g., A, B, C, and D; Fig. S3 in Supplementary materials), which are described in details by Natural Resources Conservation Service (NRCS, 2009).

2.2. Data sets for model development

The boundaries of Southeast Coasts Basin were determined based on the hydrological unit code (HUC8; ID: 03090206), delineated by the U.S. Geological Survey (USGS, 2016a). Isolated areas and barrier islands in the ocean (e.g., Miami Beach, Key Biscayne), within the extent of the HUC8 watershed, were not included in our study basin. Digital elevation models (DEMs), with a resolution of 1/3 arc-second (approximately 10 m), were obtained from the National Elevation Dataset (NED; USGS, 2016b) to represent topographical variation across the basin. Spatial variation of land cover over the basin during 2004–2013 was represented by using the 30 m 'percent developed imperviousness' data for 2006 and 2011 from the National Land Cover Database (NLCD; Fry et al., 2011; Homer et al., 2015). Soil types and properties for the subbasins were determined based on the hydrologic soil groups of the Soil Survey Geographic (SSURGO; NRCS, 2015) database, following guidelines from the national engineering handbook (NRCS, 2009) and Rawls et al. (1983).

Observations of volumetric streamflow rate for different canals and rivers during 2004–2013 were obtained from the national water information system (USGS, 2017a) and from the environmental database (called DBHYDRO) of South Florida Water Management District (SFWMD, 2017). Streamflow from 14 stations were used as the upstream boundary conditions in the model (Fig. S1 and Table S1 in Supplementary materials). Hourly water levels from the National Oceanic and Atmospheric Administration (NOAA)'s tidal station 8723214 at Virginia Key (NOAA, 2017a) were utilized as the downstream boundary conditions at the Miami River outlet. Downstream boundary conditions for other major streams were not available in close proximity. The locations of model calibrations and validations represented 6 control structures (Fig. S1). Structural attributes (e.g., number of gates, gate size, and crest elevation) and real time gate opening data for these control structures were obtained from DBHYDRO (SFWMD, 2017).

Measured data on stream cross section and bed elevation for Tamiami Canal and Miami River, as well as for their branches and tributaries, were obtained from SFWMD (see Abdul-Aziz and Al-Amin, 2015). The geometric information for rivers and canals at the northern parts of the basin were obtained from a technical report of SFWMD on the bathymetric survey of St. Lucie Estuary (Morris, 1986). Trapezoidal cross sections and bed elevation data for the remaining drainage networks were also obtained from SFWMD.

Hourly rainfall records of 2004–2013 for the 71 stations within and around the Southeast Coasts Basin (Fig. S1) were used to account for spatiotemporal variability. Rainfall data for 65 stations were collected from DBHYDRO (SFWMD, 2017), and for 6 stations from the database of national climatic data center (NOAA, 2017b). Satellite-based gridded (2 km) daily potential ET data for 2004–2013 were downloaded from USGS (USGS, 2016c) to incorporate monthly average ET rates (mm/day) in SWMM. Observed groundwater level (GWL) data for 410 stations (162 SFWMD stations and 248 USGS stations) were used to represent the interactions of surface water and groundwater in the basin (Fig. S1; SFWMD, 2017; USGS, 2017b).

2.3. Development of the hydrologic model using EPA SWMM 5.1

The U.S. EPA SWMM 5.1 is a process-based, dynamic rainfall-runoff model that integrates different components of urban hydrology, hydro-climatological variables, and land cover features (Rossman, 2015). As a first step, the large-scale basin was split into smaller subbasins, which were drained by networks of links (stream segments) and nodes (junctions). The initial set of networks was generated based on 10 m DEMs by using Arc Hydro (Maidment and Morehouse, 2002) on ESRI ArcGIS (ESRI, 2018). The subbasins and link-node networks were then modified to practically represent the complex hydrologic networks of southeast Florida (see details in Text S1 of Supplementary materials). Finally, we had 333 subbasins (with area ranging from 0.1 to 339 km^2), 434 links, and 436 nodes. Given the large area of the Southeast Coasts Basin, we did not explicitly parameterize smaller-scale drainage components such as street gutters and underground sewers with hundreds of thousands of inlets and catch basins, and tile drainage. Since our study focused on computing the generated watershed runoff rather than the local-scale flood depths, we assumed that runoff from the subbasins would eventually be drained to the larger systems of canals and rivers of the basin.

Hourly rainfall data from 71 stations were assigned to the different subbasins (Fig. S4 in Supplementary materials) based on Thiessen polygons (see Text S2 for details). Spatially averaged monthly potential ET rates (mm/day) were assigned to the model since the ET had a low spatial variability across the basin (coefficient of variation = 1.56 to 8.8% for different months). SWMM requires initial GWL as an input. We assigned dry season observations (on or near 01/01/2004) from different monitoring wells (Figs. S1 and S5) as the initial GWL for the different subbasins (Text S3 and S4). The GWL is updated dynamically in SWMM through a groundwater mass balance and interactions with the surface water (Rossman and Huber, 2016).

The overall slopes of the subbasins were determined from the percent slope raster, which was generated from the 10 m DEM by using Arc Hydro. The spatial variation of land cover (Fig. 1) across different subbasins of the Southeast Coasts Basin was represented by the temporally averaged percent imperviousness data for 2004–2013 (Fig. S6 in Supplementary materials) as inputs to SWMM. Percent imperviousness represents the proportion of a subbasin area that is made up of impervious or built surfaces (e.g., roofs, roads, parking lots, walkways). Therefore, subbasins representing highly urbanized land uses (e.g., single-family housing units, apartment complexes, commercial areas, and industrial areas) were characterized by higher percent imperviousness values (up to ~76%; Fig. S6). In contrast, subbasins representing predominantly non-urban land uses (e.g., croplands, grasslands, wetlands, and forests) had low imperviousness values (less than 10%). Based on the percent imperviousness value, a subbasin is conceptualized in SWMM with two types of functional subareas: pervious and impervious (Rossman and Huber, 2016). Runoff for the pervious subarea is computed by subtracting infiltration and ET from rainfall. Only evaporation is subtracted from rainfall to compute runoff for the impervious subarea since it does not allow infiltration and plant transpiration. However, rainfall excess (i.e., volume of rainfall available for runoff) in both types of subareas must fill the depressional storage before the onset of runoff generation.

Initial values of overland roughness coefficients and depressional storage depths of the subbasins were determined based on the recommended values in SWMM Reference Manual (Rossman and Huber, 2016) and SWMM User's Manual (Rossman, 2015). Characteristic width of the subbasins was determined based on the channel lengths and shape of the drainage areas (see Text S5). Depending on the soil types of subbasins, initial values of Green-Ampt infiltration parameters and aquifer parameters were determined based on recommendations given in SWMM Reference Manual (Rossman and Huber, 2016). Further, the model was constrained with 14 upstream boundary conditions and 1 downstream boundary condition (Fig. S1; Table S1) to account for external influence from the upstream (Lake Okeechobee, Everglades, WCAs) and tides at the downstream.

The Southeast Coasts Basin SWMM model was run at an hourly reporting time-step for continuous simulation during 2004–2013. We calibrated and validated the model with daily mean observed streamflow of, respectively, 01/01/2004–12/31/2008 and 01/01/2009–12/31/2013 at 6 different streams (Fig. S1; Table S2). Subbasin parameters such as characteristic width and overland roughness coefficients (Manning's n), infiltration parameters, aquifer parameters, coefficients (A1, A2, A3) of the lateral groundwater flow equation, and channel roughness coefficient (Manning's n) were adjusted for model calibration (Table S3). In parallel to the calibration process, we also ensured that the temporal pattern of the simulated GWL for each subbasin was realistic by bounding the lower limit of fluctuations within the vicinity of the initial (i.e., dry season) GWL.

Metrics used for model performance evaluation were the Nash-Sutcliffe Efficiency (NSE) (Nash and Sutcliffe, 1970) and the ratio of the root-mean-square error to the standard deviation of observations (RSR) (see Text S6 for details). NSE indicates the predictive efficiency of the model, whereas RSR represents the overall error in predictions. NSE = 1.0 refers to a perfect model, and NSE < 0 indicates a model that is a worse predictor than the mean of all observations as an alternative model (Moriasi et al., 2007). In contrast, RSR = 0.00–0.50, 0.50–0.60, and 0.60–0.70 indicate very good, good, and satisfactory models, respectively. A watershed hydrologic model with NSE < 0.50 and RSR > 0.70 is considered unsatisfactory. The 6 streamflow stations used for calibrations and validations of the Southeast Coasts Basin model represented control structures. Since real time gate opening data for these structures were used in the model, no streamflow was allowed when the gates had been closed. We, therefore, computed the effective NSE and RSR by excluding zero flowrate records in the observed as well as simulated time-series.

2.4. Climatic and land cover projections

We used the downscaled climatic projections of 20 Coupled Model Intercomparison Project's fifth phase (CMIP5) General Circulation Models (GCMs) (see Table S4) from the Multivariate Adaptive Constructed Analogs (MACA) dataset (Abatzoglou and Brown, 2012). This dataset provided historical climatic simulations for 1950–2005 and future projections for 2006–2099 under the Representative Concentration Pathways (RCP) 4.5 and 8.5 scenarios (IPCC, 2014b). Based on the availability of observed (gauge) hourly rainfall at 71 stations (Fig. S1), we defined the 10 years of model evaluation period (2004–2013) as our historical baseline period of 2010s. The future 10-year periods of 2050s (2044–2053) and 2080s (2076–2085), representing the mid and late 21st century, respectively, were then defined for comparative evaluations of changes in rainfall, land cover, and runoff in the study basin. The daily modeled (GCM-MACA) rainfalls were extracted for 2010s, 2050s, and 2080s at the 71 historical stations. Monthly potential ET for these periods were also obtained from the MACA dataset, which provided modeled ET using the Penman-Monteith method (Allen et al., 1998).

Based on the historical and future MACA climatic datasets, we constructed station-specific, bias-corrected future projections of rainfall by adopting a delta change factor methodology (Teutschbein and Seibert, 2012; Chen et al., 2013). MATLAB (The MathWorks, Inc., 2018) was used for constructing the rainfall projections. GCMs perform better in representing rainfall variability on the monthly scale than that on the daily scale (Zhang, 2013; Langousis et al., 2016). Therefore, relative change in rainfall between the historical 2010s and a future period (2050s, 2080s) was represented as the ratio of model-projected future monthly rainfall ($Y_{fut,\ proj}$) over model-simulated historical monthly rainfall ($Y_{hist,\ sim}$). This approach resulted in 10 ratio values (for the 10-year study periods) for each month. The monthly ratio values outside the range between a lower boundary of $Q_1 - 1.5 * IQR$ and an upper boundary of $Q_3 + 1.5 * IQR$ (Q_1 = 25th percentile; Q_3 = 75th percentile; $IQR = Q_3 - Q_1$) were identified as outliers (Tukey, 1977). The outlying ratio values were replaced with the closest boundary (i.e., upper or lower) values. The observed historical (2010s) monthly rainfall ($Y_{hist,\ obs}$) was then multiplied by the final set of change ratio values ($Y_{fut,\ proj}/Y_{hist,\ sim}$) to construct the future monthly rainfall ($Y_{fut,\ rec}$) for 2050s and 2080s. Future monthly ET scenarios were similarly constructed by incorporating the corresponding relative change ratios.

Future projections of land cover (imperviousness) were obtained from the Integrated Climate and Land-Use Scenarios (ICLUS) dataset (version 1.3.2; U.S. EPA, 2010). The ICLUS land cover projections were available for the Special Report on Emissions Scenarios (SRES) (Nakicenovic et al., 2000). Since the CMIP5 climatic projections were available for the RCP scenarios, it was necessary to relate the SRES to the RCP scenarios. In terms of atmospheric CO_2 concentrations, global radiative forcing, and global mean temperature, SRES A1FI was similar to RCP 8.5, while SRES B1 showed resemblances to RCP 4.5 (Van Vuuren and Carter, 2014). Therefore, the imperviousness projections were obtained for SRES A1 and B1. We then constructed future percent imperviousness of the subbasins using MATLAB (The MathWorks, Inc., 2018) based on the corresponding relative changes between the historical and future periods given by the ICLUS dataset. For a subbasin, ratio of the projected future imperviousness in 2050 or 2080 ($I_{fut,\ proj}$) over simulated historical imperviousness of 2010 ($I_{hist,\ sim}$) was first computed. The subbasin-level future imperviousness ($I_{fut,\ rec}$) was then constructed by multiplying this relative change ratio of imperviousness (i.e., $I_{fut,\ proj}/I_{hist,\ sim}$) with the observed historical (NLCD) imperviousness of 2010s ($I_{hist,\ obs}$). To avoid the impact of outliers in the construction of future scenarios, the maximum value of $I_{fut,\ rec}$ was set to 95%, which is typical of downtown commercial areas (Urban Drainage and Flood Control District, 2016). Further, there were a few subbasins where the ICLUS dataset either projected no relative change or relative decrease in imperviousness (i.e., $I_{fut,\ proj}/I_{hist,\ sim} \le 1$), which did not represent the persistent urbanization in southeast Florida. $I_{fut,\ rec}$ for these subbasins were estimated by using a realistic relative change ratio ($I_{fut,\ proj}/I_{hist,\ sim} > 1$) of the nearest subbasin with most similarity in observed historical land cover between them.

The constructed climatic and land cover projections under both RCP 4.5 and 8.5 were incorporated in the calibrated Southeast Coasts Basin model to obtain the potential future runoff scenarios in the 2050s and the 2080s. The constructed GCM projections of monthly rainfall were distributed to the hourly time-step as inputs to SWMM. Given the well-known lack of skills of GCMs in reproducing the smaller (than monthly) scale variability of observed rainfalls (Zhang, 2013; Langousis et al., 2016), we assumed that the hourly distribution of rainfall in the 10 years of 2050s and 2080s were similar to that in the 2010s (see Text S7 for details). The 10-year historical and future simulations of runoff were then conducted on an hourly reporting time-step over the entire basin. We assumed insubstantial changes in subbasin and stream characteristics, soil and groundwater parameters, boundary conditions, and control structure features and operations between the historical and future periods. Although this assumption may not be always accurate, it serves the purpose of scenario analyses in this study.

2.5. Sensitivity analyses

To understand runoff responses to the individual as well as simultaneous changes in the environmental drivers, we also computed the dimensionless relative sensitivity coefficients (S^*) on monthly and annual scales as follows (Abdul-Aziz et al., 2010):

$$S^* = \frac{\Delta R/R}{\Delta V/V} \quad (1)$$

where V = baseline value of the forcing or input variable (e.g., rainfall, ET, and percent imperviousness); ΔV = reference change in the forcing variable; R = baseline runoff simulated by the model; and ΔR = change in the model-simulated runoff due to the change in V.

Reference changes were applied to rainfall, ET, and imperviousness for the baseline period (2010s), and were inputted into the calibrated Southeast Coasts Basin model to compute the corresponding changes in runoff. The reference changes for these sensitivity analyses were formulated based on the future climatic and land cover projections. The four future scenarios (2050s-RCP 4.5, 2080s-RCP 4.5, 2050s-RCP 8.5, and 2080s-RCP 8.5) represented nonuniform changes in rainfall, ET, and imperviousness (Table S5 in Supplemental materials). However, we chose a uniform set of reference changes by perturbing the baseline values from −30 to +30% (with an increment of 5%) for both climatic and land cover variables so that their impacts on runoff generation could be compared. Although the ensemble average projections of all GCMs suggested overall increases in these drivers, some GCMs represented potential decreases in rainfall and ET. We, therefore, considered both increases and decreases in the drivers for sensitivity analyses — to understand the impacts of diverse changes on runoff generation mechanisms in the basin. Percent changes in runoff were computed for both individual (one-at-a-time) and simultaneous changes in rainfall, ET, and imperviousness. The individual and simultaneous changes in these variables led to 469 sensitivity scenarios for runoff. The model development and computation of runoff sensitivities and future scenarios in the Southeast Coasts Basin was summarized in a flow diagram (Fig. S7).

3. Results and discussion

3.1. Model calibrations and validations

NSE and RSR for the Southeast Coasts Basin model ranged, respectively, from 0.74 to 0.92 and 0.28 to 0.51 in calibrations and validations at the 6 stations during 2004–2013 (Fig. S8). These statistics indicated very good to excellent prediction performance of the model (Moriasi et al., 2007). The prediction performance at stations located across the basin (Fig. S1) suggested suitability of the developed model for analyzing sensitivities of historical runoff and constructing projections of future runoff scenarios under a changing climate and land cover. The baseline 10-year (2010s) mean annual runoff varied widely (5 to 1151 mm per m^2 watershed area) across the basin (Fig. S9). The corresponding baseline mean annual rainfall varied from 926 to 1627 mm across the basin, with higher (than other locations) rainfall depths in Greater Miami, Fort Lauderdale, Boca Raton, West Palm Beach, and St. Lucie areas (Fig. S4). However, the spatial variation of the baseline 2010s annual runoff mainly reflected that of the percent imperviousness (Fig. S6), with higher runoff depths in different urbanized locations (representing 30 to 76% imperviousness). For example, the north-central (e.g., West Palm Beach, Boca Raton), central (e.g., Fort Lauderdale, Hollywood, Sunrise), and the south-central (e.g., Miami, Doral, Hialeah, Homestead) regions of the basin had baseline runoff depths of 314 to 837 mm, 246 to 863 mm, and 314 to 1151 mm, respectively. Notably, the greater Miami area had the highest baseline runoff depths. In contrast, storm runoff in portions of the northern, western, and southern basin areas — representing 1 to 3% imperviousness due to croplands, pasture, grasslands, and wetlands (Fig. 1) — had much lower baseline runoff depths (18 to 45 mm).

3.2. Runoff sensitivities

3.2.1. Perturbations in rainfall

The 10-year (2004–2013) mean monthly runoff in the Southeast Coasts Basin showed notably different seasonal sensitivities to standalone changes made in hourly rainfall depths, while keeping the number and duration of rainfall events unchanged (Fig. 2a). The monthly sensitivity curves indicated nonlinear responses of runoff to perturbations in rainfall. For example, a 30% increase in rainfall led to 38 to 70% increases in runoff across different months. In contrast, a 30% decrease in rainfalls resulted in a much lower range of decreases (35 to 49%) in the corresponding monthly runoffs. On average, the annual runoff increased by 59% and decreased by 43% for, respectively, increasing and decreasing the hourly rainfall depths by 30%. The sensitivity coefficients (S^*, Eq. (1)) of runoff to the various percent changes in rainfall ranged from 1.18 to 2.35 (mean = 1.59) across the different months (Table S6 in Supplemental materials). The runoff sensitivity coefficients typically increased in magnitude with increasing rainfall.

The seasonal differences in runoff sensitivities (Fig. 2a) may be attributed to the monthly variation in rainfall depth, number of rainfall events, and ET rate (Fig. S10). According to Pathak (2001), June–September and November–April are deemed, respectively, wet and dry seasons in south Florida; May and October are transitional months. The substantially high rainfall depths and frequent rainfall events during the wet season months (Fig. S10) likely led to frequent soil saturation (despite a high ET), high antecedent soil moisture, and fast runoff generation — resulting in high runoff sensitivities. For example, the June–September runoffs increased by 57 to 70% due to 30% increases in their rainfall depths. Conversely, a 30% decrease in the wet season rainfalls resulted in 41 to 47% decreases of the monthly runoffs. Further, runoff sensitivities were higher in August–September than in June–July. This may be attributed to a higher antecedent soil moisture and faster runoff generation during the later wet months, compared to that in the early wet season (especially June, which succeeded the dry season). A similar high runoff sensitivity was also found for the transitional month of October, despite having a notably lower magnitude and frequency of rainfalls than the wet season. The high sensitivity might have been caused by a lower ET rate in October and by a presumably high antecedent soil moisture carried from the wet season.

Runoff sensitivities to rainfall were considerably lower in the dry season than the wet season (Fig. 2a). Runoff during November–April increased by 38 to 53% and decreased by 35 to 43% for, respectively, increasing and decreasing the monthly rainfalls by 30%. Contrary to the wet season, the lower runoff sensitivities during the dry season may be attributed to the lower rainfall depths and less number of rainfall events (Fig. S10). These might have led to a corresponding less frequent soil saturation (despite a lower ET, except for April), low antecedent soil moisture, and slow runoff generation in the dry season months. January runoff had the least sensitivity to changes in rainfall, apparently due to the smallest rainfall depth and lowest relative changes in baseline runoff generation (Fig. S10). In contrast, the early dry season months (November–December) experienced more frequent rainfall events. This, on top of a likely high antecedent soil moisture carried from the wet season, might have led to a faster runoff generation and a higher runoff sensitivity in November–December. The transitional month of May also had a low runoff sensitivity to changes in rainfall, similar to that of February–April, despite having a notably higher rainfall depth and frequency (Fig. S10). The low sensitivity in May might be caused by the high ET rate and the lack of antecedent soil moisture following the dry season.

3.2.2. Perturbations in ET

Runoff sensitivities to standalone changes in ET (Fig. 2b) were much lower in magnitude than that to changing rainfall. The sensitivity

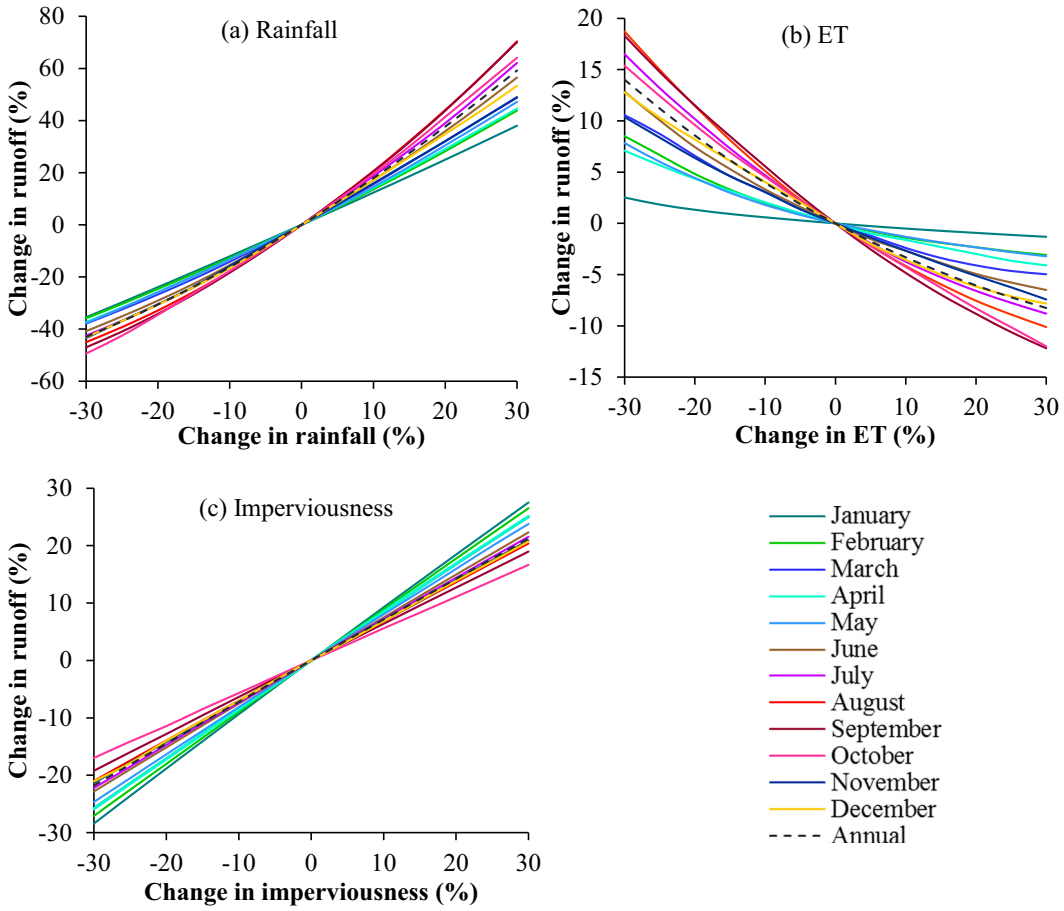

Fig. 2. Monthly and annual variation in the sensitivity of 10-year (2010s) mean runoff to perturbations in rainfall, evapotranspiration (ET), and imperviousness in the Florida Southeast Coasts Basin.

coefficients (S^*) of runoff to the various percent changes in ET ranged from −0.04 to −0.62 (mean = −0.31) across the different months (Table S7 in Supplemental materials). The runoff sensitivity coefficients typically decreased in magnitude with increasing ET. However, like rainfall perturbations, runoff sensitivities to changes in ET were nonlinear and generally higher in the wet season than that in the dry season (Fig. 2b). For example, increasing ET by 30% caused 1 to 12% decreases in the monthly runoffs and 8% decrease in the annual runoff. In contrast, runoff increased by 2.5 to 19% across different months and by 14% annually for a 30% decrease in ET. During June–October, monthly runoff decreased from 6.5 to 12% and increased from 13 to 19% for, respectively, increasing and decreasing ET by 30%. Runoff sensitivities during the early dry months (November–December) were similar to that of the early wet months (e.g., June). However, during January–May, a 30% increase in ET resulted in 1 to 5% decreases in monthly runoff, which, in turn, increased by 2.5 to 11% for a 30% decrease in ET. Overall, January runoff had the lowest sensitivity to ET, whereas September had the highest sensitivity overall (i.e., for increasing and decreasing ET).

Similar to the rainfall-runoff sensitivities, the seasonal variation in runoff sensitivities to ET were presumably caused by the seasonal variation in rainfall magnitude and frequency and in ET rates, leading to variability in antecedent soil moisture, soil saturation, and runoff generation process. For example, the higher runoff sensitivity to ET during June–October could be explained by the availability of relatively high soil moisture and higher volume of runoff generated from frequent and intense rainfalls, supporting generally a high rate of ET (except for October) (Fig. S10). In contrast, the lower runoff sensitivity during the later dry season months can be attributed to the low soil moisture and infrequent and small rainfall events, leading to a slow runoff generation to support ET that ranged from a relatively low rate in January–March to a high rate in April (Fig. S10). Further, despite having a higher magnitude and frequency of rainfall in May, the high ET rate and lack of antecedent soil moisture following the dry season might have resulted in its low runoff sensitivity to ET. Conversely, the higher runoff sensitivity in November–December than the rest of the dry season can be attributed to a faster runoff generation due to a higher magnitude and frequency of rainfall events, on top of a presumably high antecedent soil moisture carried from the wet season.

3.2.3. Perturbations in land cover

Runoff sensitivity to standalone changes in basin imperviousness was much lower than that of rainfall, but higher than ET (Fig. 2c). The sensitivity coefficients (S^*) of runoff to various percent changes in imperviousness ranged from 0.55 to 0.95 (mean = 0.76) across the different months (Table S8 in Supplemental materials). The runoff sensitivity coefficients slightly decreased in magnitude with increasing imperviousness. However, unlike rainfall and ET perturbations, runoff sensitivities to changes in imperviousness were mostly linear, and were higher in the dry season than that in the wet season (Fig. 2c). The monthly runoffs both increased and decreased by 17 to 28% for, respectively, increasing and decreasing the imperviousness of all subbasins by 30%, for example. On average, the annual runoff changed (increased or decreased) by 21 to 22% for the corresponding changes in the imperviousness by 30%. Runoff during June–October changed by 17 to 23%, whereas runoff during November–May changed by 21 to 28% for a 30% change in the basin imperviousness. Compared to the runoff changes due to the rainfall perturbations (Section 3.2.1), the results indicated more than 2 to 3 times stronger control of climate (rainfall) on runoff than imperviousness in

Table 1
Percent changes of mean annual runoff under concurrent perturbations in rainfall and imperviousness in the Florida Southeast Coasts Basin.

Change in imperviousness (%)	Change in rainfall (%)												
	−30	−25	−20	−15	−10	−5	0	5	10	15	20	25	30
−30	−58	−53	−48	−42	−36	−29	−22	−14	−6	3	12	22	32
−25	−56	−51	−45	−39	−33	−26	−18	−10	−2	7	16	26	36
−20	−53	−48	−42	−36	−29	−22	−15	−6	2	11	21	31	41
−15	−51	−45	−39	−33	−26	−19	−11	−3	6	15	25	35	46
−10	−48	−42	−36	−30	−23	−15	−7	1	10	19	29	39	50
−5	−45	−40	−33	−27	−19	−12	−4	5	14	23	33	44	55
0	−43	−37	−31	−24	−16	−8	0	9	18	28	38	48	59
5	−40	−34	−28	−21	−13	−5	4	12	22	32	42	53	64
10	−38	−32	−25	−18	−10	−2	7	16	26	36	46	57	68
15	−35	−29	−22	−15	−7	2	11	20	30	40	50	61	73
20	−33	−26	−19	−11	−3	5	14	24	33	44	54	66	77
25	−31	−24	−16	−8	0	9	18	27	37	48	59	70	82
30	−28	−21	−14	−5	3	12	21	31	41	52	63	74	86

Note: Positive sign indicates increase, while negative indicates decrease.

Table 2
Percent changes of mean annual runoff under concurrent perturbations in rainfall and evapotranspiration (ET) in the Florida Southeast Coasts Basin.

Change in ET (%)	Change in rainfall (%)												
	−30	−25	−20	−15	−10	−5	0	5	10	15	20	25	30
−30	−37	−30	−22	−14	−5	4	14	24	35	46	57	69	81
−25	−39	−31	−24	−16	−7	2	11	21	31	42	53	65	77
−20	−40	−33	−26	−18	−9	−1	9	18	28	39	50	61	73
−15	−41	−34	−27	−19	−11	−3	6	16	25	36	47	58	69
−10	−42	−35	−28	−21	−13	−5	4	13	23	33	43	54	66
−5	−42	−36	−30	−22	−15	−7	2	11	20	30	40	51	62
0	−43	−37	−31	−24	−16	−8	0	9	18	28	38	48	59
5	−43	−38	−31	−25	−18	−10	−2	7	16	25	35	45	56
10	−44	−38	−32	−26	−19	−11	−3	5	14	23	33	43	53
15	−44	−39	−33	−26	−20	−12	−5	3	12	21	30	40	51
20	−44	−39	−33	−27	−21	−14	−6	2	10	19	28	38	48
25	−45	−39	−34	−28	−21	−15	−7	1	9	17	26	36	46
30	−45	−40	−34	−28	−22	−15	−8	−1	7	16	25	34	44

Note: Positive sign indicates increase, while negative indicates decrease.

the overall highly urbanized Florida Southeast Coasts Basin. The stronger sensitivities of dry season runoff to imperviousness perturbations indicated a more prominent role of imperviousness in runoff generation than that during the wet season, given typically lower depths and frequency of rainfall and lower ET in the dry season.

3.2.4. Concurrent climatic and land cover sensitivities

Concurrent changes in rainfall and imperviousness, as well as in rainfall and ET, led to stronger nonlinear responses of runoff than the linear summation of their standalone (i.e., one-at-a-time) individual effects (Tables 1 and 2). For example, when both rainfall and imperviousness were simultaneously increased by 30%, the annual basin runoff increased by 86%, which was 6 percentage points higher than the linear summation of their standalone individual contributions (i.e., 59% + 21%; Table 1). Further, a concurrent 30% increase in both rainfall and ET increased the annual basin runoff by 44%, which was 7 percentage points lower than the linear summation of their standalone individual contributions (Table 2). However, runoff responses to concurrent changes in both imperviousness and ET were mostly linear — similar to that obtained by summing their standalone individual contributions (Table 3). The results reemphasized a stronger role of rainfall, quicker soil saturation,

Table 3
Percent changes of mean annual runoff under concurrent perturbations in evapotranspiration (ET) and imperviousness in the Florida Southeast Coasts Basin.

Change in imperviousness (%)	Change in ET (%)												
	−30	−25	−20	−15	−10	−5	0	5	10	15	20	25	30
−30	−7	−10	−13	−15	−18	−20	−22	−24	−25	−27	−28	−29	−30
−25	−4	−7	−9	−12	−14	−16	−18	−20	−21	−23	−24	−25	−26
−20	0	−3	−6	−8	−10	−13	−15	−16	−18	−19	−21	−22	−23
−15	3	0	−2	−5	−7	−9	−11	−13	−14	−16	−17	−18	−19
−10	7	4	1	−1	−3	−5	−7	−9	−11	−12	−13	−14	−15
−5	10	8	5	3	0	−2	−4	−5	−7	−8	−10	−11	−12
0	14	11	9	6	4	2	0	−2	−3	−5	−6	−7	−8
5	18	15	12	10	8	5	4	2	0	−1	−2	−4	−5
10	21	18	16	13	11	9	7	5	4	2	1	0	−1
15	25	22	19	17	15	13	11	9	7	6	5	4	2
20	28	25	23	20	18	16	14	13	11	10	8	7	6
25	32	29	26	24	22	20	18	16	14	13	12	11	10
30	35	32	30	27	25	23	21	20	18	17	15	14	13

Note: Positive sign indicates increase, while negative indicates decrease.

and faster runoff generation in driving runoff sensitivities in the coastal-urban environments.

3.3. Future runoff projections

3.3.1. Runoff projections under changing climate

Simulated ensemble mean runoff depths, in response to the climatic (rainfall and ET) projections of 20 GCMs, suggested high (on spatial average, 142 to 267 mm per m^2 basin area) increases in the 10-year mean annual storm runoff for the Southeast Coasts Basin across the RCP scenarios by 2050s and 2080s (Fig. 3), relative to the 2010s (Fig. S9). The corresponding projected ensemble mean increases in the 10-year mean annual rainfall ranged from 174 to 407 mm under different future scenarios (Fig. S11a). Spatial variation in the projected increases of rainfall led to higher (than other locations) projected increases of storm runoff in different urbanized locations. The higher runoff increases were more notable across a long stretch from the south-central to the north-central region of the basin (spatial mean of 241 to 437 mm), including the major cities of Miami, Fort Lauderdale, and West Palm Beach (Figs. 1, 3a). Much of the northern, western, and southern basin areas would experience relatively lower increases in runoff depth (spatial mean of 30 to 45 mm; Fig. 3a), despite receiving relatively high projected increases in rainfall. These areas were primarily characterized by croplands, pasture, grasslands, and wetlands (Fig. 1). However, the low increases in runoff depths represented high relative increases (246 to 364%) due to the corresponding lower baseline runoffs in these natural and unbuilt areas (Fig. S9), and can therefore be hydrologically impactful. Overall, the highest runoff increases were observed for the 2080s-RCP 4.5 scenario (Fig. 3a), resulting from the highest rainfall increases (Fig. S11a) across the basin. In contrast, the lowest increases in the annual runoff resulted under the 2080s-RCP 8.5 scenario — in response to the corresponding lowest ensemble mean increases in rainfall and the highest increases in ET (Fig. S11a, Table S5).

Based on the total basin runoff, higher relative changes in the 10-year mean runoffs were observed for the dry season and transitional months (October–May; 92 to 165% increases on average) than that for the wet season (June–September; from 13% decrease to 66% increase) under different future scenarios (Fig. 4a). The seasonal pattern contrasted with the results of runoff sensitivity analysis to rainfall perturbations by up to 30% (Section 3.2.1). The reverse seasonal pattern of the projected future runoff changes was primarily caused by the much higher relative changes in the projected rainfall

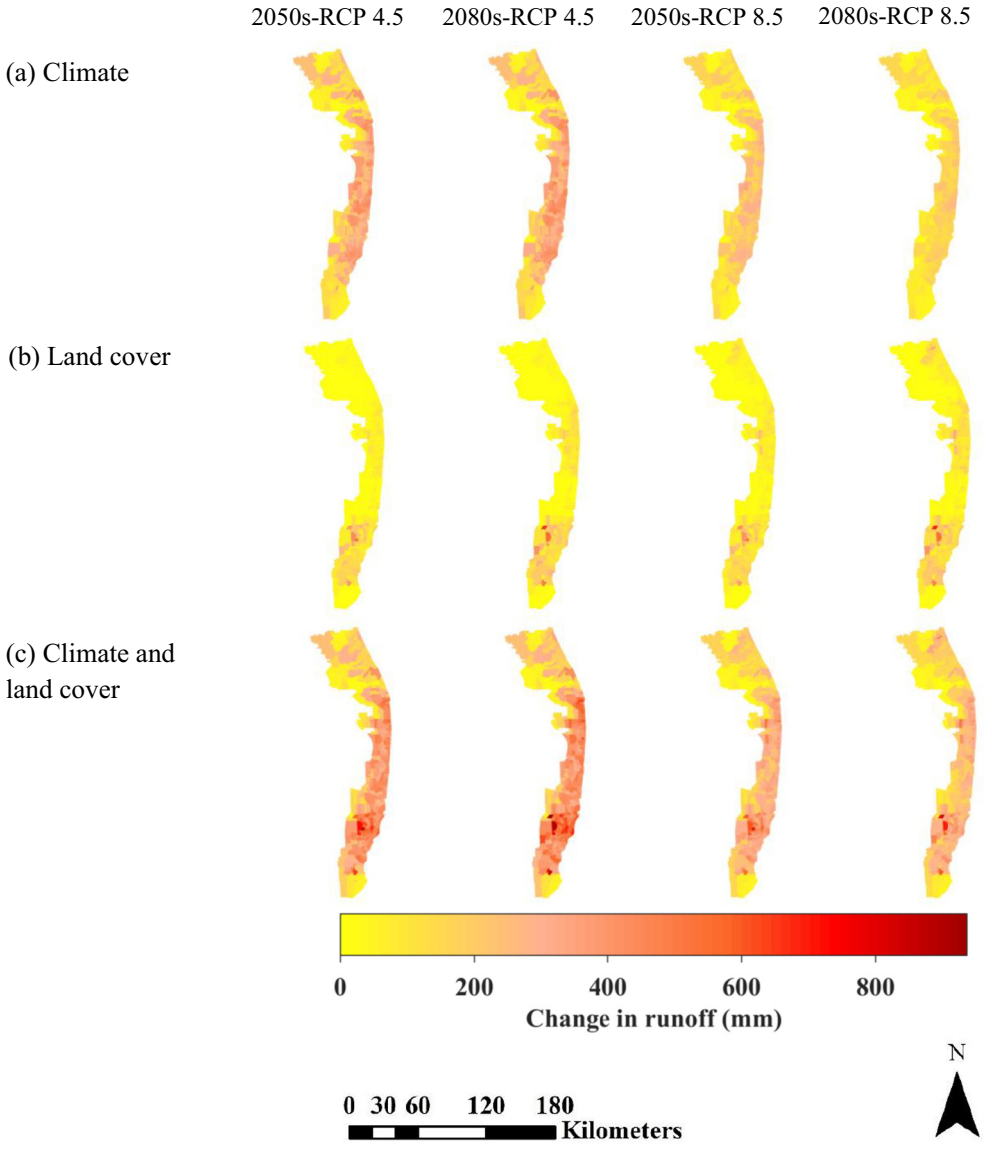

Fig. 3. Spatial variation of the predicted changes in 10-year mean annual runoff depth due to the projected changes in (a) climate, (b) land cover, and (c) both climate and land cover under different future scenarios in the Florida Southeast Coasts Basin.

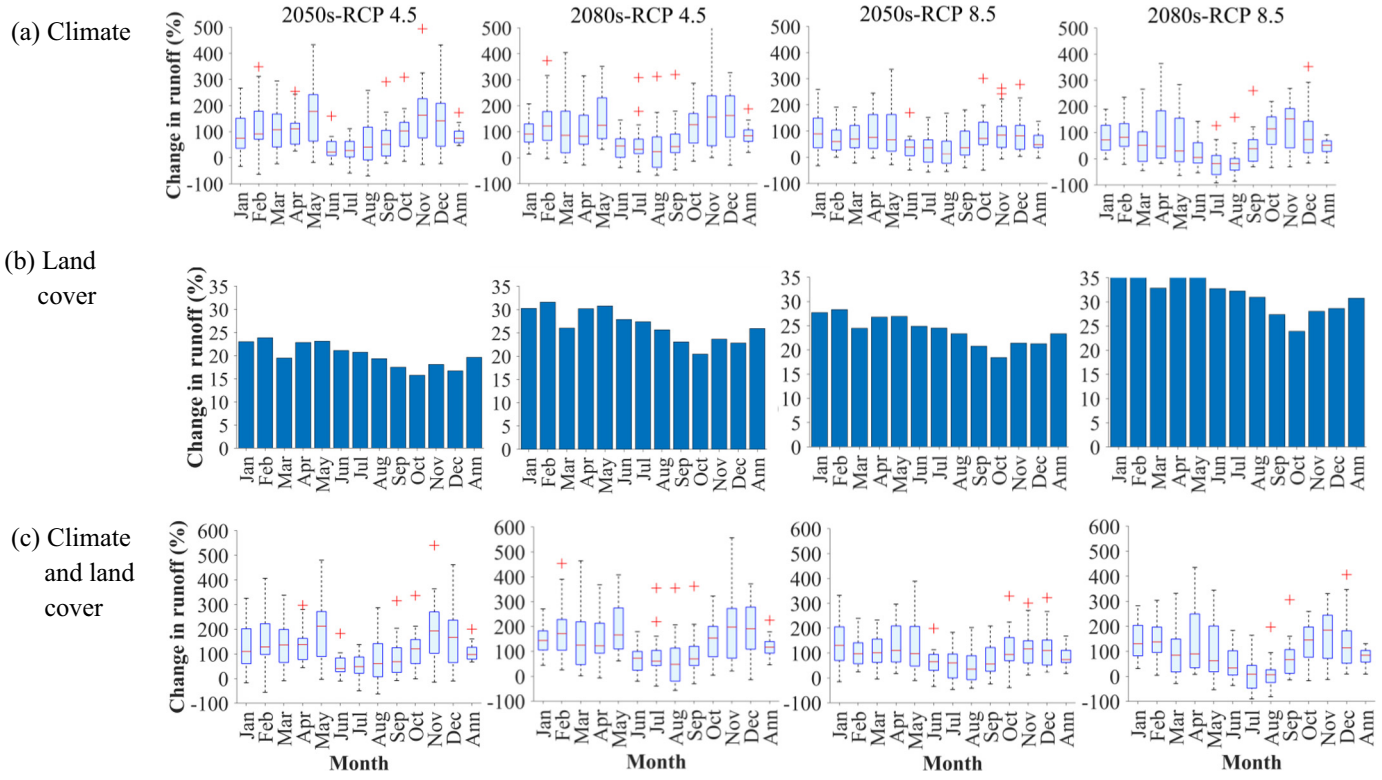

Fig. 4. Percentage changes in 10-year mean monthly and annual runoff under the projected changes in (a) climate, (b) land cover, and (c) both climate and land cover for different future scenarios in the Florida Southeast Coasts Basin. For (a) and (c), the box-whiskers represent variations in runoff change across the general circulation models (GCMs); the lower, intermediate, and upper horizontal lines in the boxes indicate 25th, 50th, and 75th percentiles; plus signs indicate extreme outliers. Jan: January; Feb: February; Mar: March; Apr: April; Jun: June; Jul: July; Aug: August; Sep: September; Oct: October; Nov: November; Dec: December; Ann: Annual.

(18 to 70% increase) during October–May than during June–September (ranging from 22% decrease to 22% increase; Fig. S12a). Based on the ensemble model average, the overall basin rainfall was projected to increase by approximately 30%, 29%, 20%, and 13%, respectively, under the 2080s-RCP 4.5, 2050s-RCP 4.5, 2050s-RCP 8.5, and 2080s-RCP 8.5 scenarios (Table S5). The basin ET was also projected to increase by 8.5% (2080s-RCP 8.5), 4.6% (2050s-RCP 8.5), 4.5% (2080s-RCP 4.5), and 2.9% (2050s-RCP 4.5). The projected changes in climate generally caused high ensemble mean increases in the annual runoff volume under all scenarios: 2080s-RCP 4.5 (87%), 2050s-RCP 4.5 (83%), 2050s-RCP 8.5 (60%), and 2080s-RCP 8.5 (47%) (Table 4). The smaller ensemble mean increases in annual basin runoff under the RCP 8.5 scenarios stemmed from the higher mix of projected increases and decreases in runoff than the RCP 4.5 scenarios (Fig. 4a). This, in turn, was mainly caused by the corresponding higher mix of projected increases and decreases in annual rainfall given by the GCMs under the RCP 8.5 scenarios (Fig. S12a). The smallest runoff increase was observed under 2080s-RCP 8.5, since it had the largest number of GCMs projecting decreases in basin rainfall.

Table 4
Potential future increases (model-projected ensemble average) in the mean annual runoff volume for the Florida Southeast Coasts Basin under different scenarios of changing climate and/or land cover, relative to the baseline period of 2010s.

Changing drivers/scenarios	Projected increases in runoff (%)			
	2050s-RCP 4.5	2080s-RCP 4.5	2050s-RCP 8.5	2080s-RCP 8.5
Climate	83	87	60	47
Land cover	20	26	23	31
Climate and land cover	106	118	86	80

3.3.2. Runoff projections under changing land cover

Commensurate with the increasing urbanization and developments, increases in surface imperviousness were projected throughout the Southeast Coasts Basin under all scenarios (Fig. S11b). However, the overall (basin-average) 7 to 10 percentage points increase in imperviousness led to much lower increases (70 to 98 mm per m^2 basin area; Fig. 3b) in mean annual storm runoff depth than climatic changes by the 2050s and 2080s, relative to the 2010s. The basin-wide highest and lowest increases in runoff due to the corresponding increases in imperviousness were obtained under the 2080s-RCP 8.5 and 2050s-RCP 4.5 scenarios, respectively. Across the four future scenarios, 14 to 22 percentage points (spatial mean) increases in imperviousness (Fig. S11b) caused 155 to 233 mm (spatial mean) increases in 10-year mean annual runoff (Fig. 3b) at urban centers (e.g., Fort Pierce, Port St. Lucie, Jupiter, West Palm Beach, Boca Raton, Doral, Hialeah, Miami, Homestead). Further, runoff increases of 177 to 337 mm (spatial mean) at the northern, western, and southern basin areas were caused by the projected conversion of croplands, pasture, grasslands, and wetlands (Fig. 1) to more impervious land covers (on average, 20 to 40 percentage points increases in imperviousness; Fig. S11b).

Potential land cover change impacts on the total basin runoff were overall slightly more pronounced during the dry season than the wet season (Fig. 4b). Under different future scenarios, monthly basin runoff was projected to increase by 17 to 37% and 16 to 33% during November–May and June–October, respectively. The projected seasonal pattern was consistent with the findings of sensitivity analysis (Section 3.2.3). Based on the average, the overall basin imperviousness was projected to increase by approximately 36%, 31%, 28%, and 25%, respectively, under the 2080s-RCP 8.5, 2080s-RCP 4.5, 2050s-RCP 8.5, and 2050s-RCP 4.5 scenarios (Table S5). The potential land cover changes would lead to moderate increases in basin-scale runoff volume under 2080s-RCP 8.5 (31%), followed by 2080s-RCP 4.5 (26%), 2050s-RCP 8.5 (23%), and 2050s-RCP 4.5 (20%) (Table 4). The much lower potential runoff

increases under land cover changes than that under climatic changes further underlined the overall dominance of climate in runoff generation in the Southeast Coasts Basin.

3.3.3. Runoff projections under both changing climate and land cover

Simultaneous projected changes in climate and land cover produced more widespread and higher increases in storm runoff depth (244 to 367 mm per m^2 basin area) in the Southeast Coasts Basin than that due to the standalone climatic or land cover changes under all four scenarios (Fig. 3c), relative to the 2010s. High potential ensemble increases in 10-year mean annual runoff — caused by concurrent moderate to high ensemble mean increases in rainfall and impervious cover (Fig. S11a, b) — were noted at and around majority of the urban centers across the basin by 2050s to 2080s. For example, future runoff increases (spatial average) of 354 to 512 mm, 224 to 375 mm, and 392 to 610 mm were projected, respectively, across the north-central (e.g., West Palm Beach, Boca Raton), central (e.g., Fort Lauderdale, Hollywood, Sunrise), and the south-central (e.g., Miami, Doral, Hialeah, Homestead) regions of the basin. Remarkably, the greater Miami area (Figs. 1, 3c) would experience the highest increases in runoff under all four scenarios. Furthermore, spatial mean runoffs in portions of the northern, western, and southern basin areas — representing croplands, pasture, grasslands, and wetlands (Fig. 1) — were projected to increase by 59 to 77 mm (218 to 306% increase relative to the 2010s) by 2050s to 2080s (Fig. 3c). Overall, the spatial patterns of projected runoff increases under concurrent climatic and land cover changes were dominated by that under climatic changes (Fig. 3a). Therefore, the basin-wide higher and lower increases in runoff under the combined changes were noted, respectively, under the RCP 4.5 and RCP 8.5 scenarios.

The combined changes in climatic and land cover variables produced higher relative increases in future runoff volume during the dry season and transitional months than that during the wet season (Fig. 4c). Monthly basin runoffs were projected to increase by 100 to 201% during October–May and by 10 to 90% during June–September under the different scenarios. The seasonal patterns of predicted runoff changes appeared to be largely reflective of the seasonal variation in projected changes in rainfall (Fig. S12a). The 10-year mean annual basin runoff volume would increase by 118%, 106%, 86%, and 80% under the 2080s-RCP 4.5, 2050s-RCP 4.5, 2050s-RCP 8.5, and 2080s-RCP 8.5 scenario, respectively (Table 4). The smaller ensemble mean runoff increases under the two RCP 8.5 scenarios were caused by the corresponding higher mix of projected increases and decreases in annual rainfall given by the GCMs (Fig. S12a). Consistent with the sensitivity analysis (Section 3.2.4), the relative basin runoff increases in the 2050s and 2080s under concurrent climatic and land cover changes were higher than the superposed runoff increases under standalone changes in climate and land cover. Based on the basin-scale changes, 2050s-RCP 4.5 and 2080s-RCP 4.5 provided the most critical future runoff scenario for, respectively, the near term and longer term infrastructure design, construction, and maintenance.

3.4. Comparative synthesis of findings with existing literature

The overall runoff sensitivities to climatic and land cover changes in our current study on the large-scale Southeast Coasts Basin were similar to that in the much smaller scale study of Abdul-Aziz and Al-Amin (2015) on Miami River Basin, supporting scale-transition of the findings. However, some discrepancies were noted in the dry season months of November and December, which had high runoff sensitivities to rainfall in the Miami River Basin. Apart from the stark difference in the spatial scales of the two studies, it is also worth mentioning here that Abdul-Aziz and Al-Amin (2015) mainly focused on evaluating the runoff sensitivities using historical data of one year (2010). In contrast, our current study evaluated the potential changes in runoff by directly incorporating GCMs-projected climatic changes and land cover projections, in addition to the sensitivity analysis, using the 10-year periods of 2010s, 2050s, and 2080s.

The occasional differences in rainfall-runoff sensitivities between the current study and that by Abdul-Aziz and Al-Amin (2015) were likely contributed by the associated variation in temporal rainfall distributions and surface imperviousness, which may modulate the response of surface runoff to changes in rainfall. Previous studies (e.g., Ali and Abtew, 1999) reported spatial variation in annual percentage of dry season rainfall over south Florida. Seasonal rainfall distributions can also vary due to the periodic influence of large-scale circulations such as El Niño-Southern Oscillation (ENSO), Pacific Decadal Oscillation (PDO), Atlantic Multi-decadal Oscillation (AMO), North Atlantic Oscillation (NAO), Arctic Oscillation (AO), sea-breeze convection, and tropical storms/hurricanes (Schmidt et al., 2001; Obeysekera et al., 2011; Abdul-Aziz and Al-Amin, 2015). The monthly rainfall distributions and the runoff sensitivities may, therefore, vary in different years and locations.

Outcomes of the sensitivity analyses and the future runoff scenarios for the Southeast Coasts Basin reinforced the findings across different regions of the globe. The runoff in the Southeast Coasts Basin was more sensitive to rainfall than ET on both monthly and annual scales (Fig. 2a, b). Berghuijs et al. (2017) obtained higher sensitivity of runoff to changing rainfall than to changing ET globally. Chiew and McMahon (2002) reported an amplified annual runoff variation of −5 to +15% (negative and positive signs indicating decrease and increase, respectively) in response to −4 to +7% (respectively) changes in annual rainfall for the northeast coast of Australia, which has a tropical climate (ORNL, 2017). In our sensitivity analysis experiments, we found a proportionally similar responses (−43 to +59% changes) in mean annual runoff for −30 to +30% (respectively) changes in the mean annual rainfall during 2004–2013 (Fig. 2a). Similarly, the GCMs-projected 13 to 30% increases in annual basin rainfall (Table S5) led to 47 to 87% increases in annual basin runoff by 2050s and 2080s under different scenarios (Table 4).

Our results for the Florida Southeast Coasts Basin suggested that climatic (rainfall) change would be substantially more impactful on basin-scale runoff generation than land cover change under different future scenarios and time-frames. This is consistent with the existing literature on other regions around the world (e.g., Öztürk et al., 2013; Sunde et al., 2018; Wang and Stephenson, 2018) — indicating climate as the principal driver of potential future changes in runoff, while land cover changes were also important contributors. Olivera and DeFee (2007) attributed 77% increase in annual runoff in the Whiteoak Bayou watershed of Texas, USA to 181% growth in the impervious area. In comparison, our perturbations-based sensitivity analyses suggested 21% increase in mean annual runoff for a 30% increase in imperviousness (Fig. 2c). Further, our future projections suggested 20 to 31% increases in annual runoff due to 25 to 36% (respectively) increases in imperviousness under different scenarios (Tables 4 and S5). Our runoff sensitivity analysis and future runoff projections also underlined nonlinear responses of runoff when both changing climate and land cover were considered in hydrologic simulations for the Southeast Coasts Basin — reinforcing the message from the previous studies (e.g., Abdul-Aziz and Al-Amin, 2015; Hovenga et al., 2016).

3.5. Implications for water resources planning and management

Future shifts in runoff under projected climatic and land cover changes can have drastic hydrologic and environmental impacts in the Southeast Coasts Basin. High ensemble mean increases in monthly and annual runoff by the 2050s and 2080s (Figs. 3 and 4) would lead to potentially higher than average water levels in the drainage streams and flood control systems over southeast Florida. The runoff projections suggested a substantially higher risk for freshwater flooding and stream water pollutions in major urban centers (e.g., Greater Miami, Fort Lauderdale, Boca Raton, West Palm Beach, Jupiter, Fort Pierce) throughout the basin. Given the non-linear watershed hydrologic processes, it would be imperative to incorporate storm runoff responses under

concurrent climatic and land cover changes, instead of just superposing their isolated impacts, in these complex coastal-urban environments. The remarkably high ensemble mean increases in watershed runoff calls for drastic upgradations of existing stormwater drainage infrastructure through retrofitting, rehabilitations, and new constructions, as appropriate. Furthermore, the potential increases in urban and agricultural runoff would result in much enhanced pollutant (e.g., nutrients) discharges to the downstream waters such as the Indian River Lagoon, St. Lucie Estuary, and Biscayne Bay. Increase in nutrient concentrations can promote harmful algal blooms in these estuarine waterbodies. High algal blooms, in turn, would endanger oyster reefs, sea grasses, and many other marine species by producing harmful toxins, blocking the sunlight, and depleting dissolved oxygen (Boesch et al., 1997). Excessive nutrient loading, high turbidity, and low salinity in the freshwater influx may also lead to bleaching and subsequent death of the coral reefs of the adjacent estuaries (e.g., St. Lucie Estuary; see Lapointe et al., 2012).

3.6. Limitations, caveats, and uncertainties

We did not report the consideration of potential sea level rise (SLR) in constructing the sensitivity and future scenarios of stormwater runoff for the Southeast Coasts Basin. However, based on the projected SLR scenarios for southeast Florida (SFRCCC Sea Level Rise Work Group, 2015), we investigated the potential impacts of SLR on the basin-scale stormwater budget (pluvial runoff generated by rainfall accumulations). In our modeling experiments, we conducted these analyses by first fixing the observed or modeled water level (if observations were not available) at stream outlets during the baseline 2010s period as the downstream boundary conditions. SWMM was then run by increasing the boundary conditions by the recommended scenarios of SLR (25 to 150 cm), relative to the 2010s water level. The projected SLR scenarios did not appreciably affect runoff generation during the 10-year period in the basin, except for small (i.e., line-shaped) areas adjacent to the stream outlets to the ocean. Furthermore, we evaluated the impacts of potential changes in the upstream boundary conditions for rivers and canals that had originated outside the Southeast Coasts Basin (e.g., from Lake Okeechobee). The boundary conditions were perturbed by −30 (decrease) to +30% (increase), with an increment of 5%. The perturbation experiments did not notably change runoff depth during 2010s in the basin, except for small areas adjacent to the upstream boundaries. Overall, the basin-scale storm runoff of 2010s was not notably sensitive to the projected SLR or to the perturbations in the upstream boundary conditions. Therefore, it was reasonable to mainly construct the future scenarios of basin runoff based on the projected changes in climate (rainfall, ET) and land cover (imperviousness).

In constructing the runoff scenarios of 2050s and 2080s for the Southeast Coasts Basin, our study assumed similar drainage network and stream hydrology between the historical and future periods. Subject to the poor skills of GCMs in accurately reproducing hourly rainfalls, we used the hourly observed distributions of rainfall within a month from the 2010s to distribute the projected total rainfall for the corresponding month to different hours for 2050s and 2080s. Given the large area of the basin, we did not explicitly parameterize the hundreds of thousands of local stormwater management structures such as street inlets, underground sewers, catch basins, and tile drainage in our model. Instead, runoff from the subbasins was assumed to ultimately drain into the rivers and canals. These may be considered as caveats of our study given that any future changes in rainfall hyetograph, stormwater management structures, and drainage network are inherently expected to influence the process of soil saturation, runoff generation, and mass transport.

Climate in southeast Florida often experiences seasonal anomalies driven by the large-scale ocean-atmospheric phenomena such as PDO, AMO, NAO, AO, ENSO, sea-breeze related convection, and tropical storms/hurricanes (Obeysekera et al., 2011; Abdul-Aziz and Al-Amin, 2015). Limited abilities of the CMIP5 GCMs to parameterize these phenomena have been discussed in previous studies (e.g., Zhao et al., 2017; Lu et al., 2018). Any future runoff projections would be prone to the concomitant uncertainties in the modeled and projected rainfalls. Furthermore, disagreement in the projections of rainfall and ET among the GCMs resulted in a wide range of possible future runoff scenarios. The high uncertainty of the ICLUS land cover projections is also a caveat given the dynamic human-landscape interactions. We, therefore, employed the ensembled runoff projections to obtain an overall, generalized perspective on the impacts of changing climate and land cover on the basin-scale runoff.

4. Conclusions

We determined the individual as well as the synergistic controls of climatic and land cover changes on stormwater runoff regimes in complex coastal-urban environments, considering Florida Southeast Coasts Basin as the study area. A large-scale (7117 km^2) mechanistic hydrologic model was developed for this basin using U.S. EPA SWMM 5.1. The model was calibrated and validated (NSE = 0.74 to 0.92, RSR = 0.28 to 0.51) with daily streamflow observations for the historical 10-year period of 2010s (2004–2013). The basin-scale storm runoff had notably different seasonal sensitivities to standalone perturbations (−30 to +30%, with 5% increments) in rainfall, ET, and imperviousness. The runoff sensitivities to rainfall and ET were strongly nonlinear across the range of perturbations, whereas the sensitivities to imperviousness were mostly linear. Overall, the sensitivity scenarios suggested that climatic changes would be substantially more impactful on storm runoff generation than land cover changes in these coastal-urban environments. Based on annual averages, rainfall had approximately 2.5 and 5 times stronger control on runoff than that of imperviousness and ET, respectively. Further, stronger nonlinear responses of runoff were obtained due to concurrent changes in climate and land cover than the linear summations of their individual effects.

Based on the climatic projections of 20 GCMs and land cover projections of ICLUS, the Southeast Coasts Basin would experience high ensemble increases in 10-year mean annual storm runoff by 2050s (2044–2053) and 2080s (2076–2085), relative to the 2010s. Higher runoff increases were noted at and around majority of the urban centers across the basin (e.g., Miami, Fort Lauderdale, West Palm Beach, and Port St. Lucie). Remarkably, the highest potential runoff increases were projected in the greater Miami area. However, much of the northern, western, and southern basin areas — currently representing croplands, pasture, grasslands, and wetlands — would experience a substantial relative increase in runoff; primarily due to their conversions to more impervious (e.g., built-up) land uses. On the basin-scale average, the projected climatic changes would lead to high increases (47 to 87%) in annual storm runoff by the middle through the end of the 21st century. In contrast, the projected land cover changes would cause moderate increases (20 to 31%) in the annual runoff. However, under the projected concurrent changes in climate and land cover, the annual basin runoff would increase by 80 to 118%. The relative increases in runoff due to the combined changes in climate and land cover were higher during the dry season and transitional months (October–May) than the wet season (June–September). The seasonal variation of the projected changes in rainfall and runoff were nearly identical. The basin-scale runoff increases and their seasonal patterns reiterated the predominant climatic control on the storm runoff and associated high vulnerability in the coastal-urban environments.

The study evaluated the research hypothesis that climatic and land cover changes would overall substantially increase stormwater runoff in tropical/sub-tropical coastal-urban environments. The projected runoff increases across the Southeast Coasts Basin by 2050s and 2080s indicated the critical areas of potentially increased flooding risks and water quality impacts in streams and the surrounding ecosystems. Major upgradations of existing stormwater drainage infrastructure should be pursued to convey the projected high increases in runoff. Appropriate

management and remediation measures should also be undertaken to alleviate the potentially enhanced pollutant discharges from urban and agricultural areas to the downstream waters. The findings are particularly relevant in areas of high latitudes and wet tropical/subtropical regions that would experience increases in rainfall and urbanization (IPCC, 2014a). Our findings may, therefore, provide important guidance for development, improvement, and management of stormwater drainage infrastructure to achieve sustainability and resilience in southeast Florida and similar coastal built environments around the world.

CRediT authorship contribution statement

Abdul-Aziz conceptualized the research idea and designed the methodology. Huq and Abdul-Aziz conducted the analyses and summarized the results. Both authors contributed to the writing. Abdul-Aziz administered the projects funding the research and supervised Huq. All authors have read and agreed to the published version of the manuscript.

Declaration of competing interest

The authors declare that they have no known competing financial interests or personal relationships that could have appeared to influence the work reported in this paper.

Acknowledgments

The research was funded by a National Science Foundation (NSF) Critical Resilient Interdependent Infrastructure Systems and Processes (CRISP 2.0) Award to Dr. Omar I. Abdul-Aziz (NSF CMMI Award #1832680), and by the "Florida Public Hurricane Loss Model Enhancements" project's freshwater flood modeling award to Dr. Omar I. Abdul-Aziz. The research on climate and land cover change impacts on stormwater runoff was exclusively funded by the NSF project. The findings and conclusions of this research are those of the authors, and do not necessarily reflect the views of NSF and the State of Florida or any of its sub-agencies. We also thank the seven anonymous reviewers for their insightful comments on the primary manuscript.

Notations

The following symbols were used in this paper:

$Y_{hist,\ obs}$	observed historical monthly climatic (i.e., rainfall and ET) variable
$Y_{hist,\ sim}$	simulated historical monthly climatic variable
$Y_{fut,\ proj}$	projected future monthly climatic variable
$Y_{fut,\ rec}$	reconstructed future monthly climatic variable
$I_{hist,\ obs}$	observed historical imperviousness
$I_{hist,\ sim}$	simulated historical imperviousness
$I_{fut,\ proj}$	projected future imperviousness
$I_{fut,\ rec}$	reconstructed future imperviousness
Q_1	25th percentile
Q_3	75th percentile
IQR	$Q_3 - Q_1$
S^*	dimensionless relative sensitivity coefficient
V	baseline value of the forcing variable or parameter (e.g., rainfall, ET, and percent imperviousness)
ΔV	change in the forcing variable
R	baseline runoff simulated by the model
ΔR	change in model-simulated runoff

Appendix A. Supplementary materials

Supplementary materials to this article can be found online at https://doi.org/10.1016/j.scitotenv.2021.146017.

References

Abatzoglou, J.T., Brown, T.J., 2012. A comparison of statistical downscaling methods suited for wildfire applications. Int. J. Climatol. 32 (5), 772–780. https://doi.org/10.1002/joc.2312.

Abdul-Aziz, O.I., Al-Amin, S., 2015. Climate, land use and hydrologic sensitivities of stormwater quantity and quality in a complex coastal-urban watershed. Urban Water J. 13 (3), 302–320. https://doi.org/10.1080/1573062X.2014.991328.

Abdul-Aziz, O.I., Wilson, B.N., Gulliver, J.S., 2010. Two-zone model for stream and river ecosystems. Hydrobiologia. 638 (1), 85–107. https://doi.org/10.1007/s10750-009-0011-7.

Ali, A., Abtew, W., 1999. Regional rainfall frequency analysis for central and south Florida. Technical Publication WRE 380. South Florida Water Management District, West Palm Beach, FL, USA.

Allen, R.G., Pereira, L.S., Raes, D., Smith, M., 1998. Crop Evapotranspiration: Guidelines for Computing Crop Water Requirements. FAO Irrigation and Drainage Paper. vol. 56. Food and Agriculture Organization, Rome, Italy. http://www.fao.org/docrep/x0490e/x0490e00.htm.

Al-Safi, H.I.J., Kazemi, H., Ranjan Sarukkalige, P., 2020. Comparative study of conceptual versus distributed hydrologic modelling to evaluate the impact of climate change on future runoff in unregulated catchments. J. Water Clim. Chang. 11, 341–366. https://doi.org/10.2166/wcc.2019.180.

Al-Safi, H.I.J., Sarukkalige, P.R., 2019. Hydrological impacts of climate change on the future streamflow of three unregulated catchments of the Australian hydrologic reference stations. Int. J. Hydrol. Sci. Technol. 9, 366–398. https://doi.org/10.1504/IJHST.2019.102420.

Berghuijs, W.R., Larsen, J.R., Van Emmerik, T.H., Woods, R.A., 2017. A global assessment of runoff sensitivity to changes in precipitation, potential evaporation, and other factors. Water Resour. Res. 53 (10), 8475–8486. https://doi.org/10.1002/2017WR021593.

Bharat, S., Mishra, V., 2020. Runoff sensitivity of Indian sub-continental river basins. Sci. Total Environ. 142642. https://doi.org/10.1016/j.scitotenv.2020.142642.

Boesch, D.F., Anderson, D.M., Horner, R.A., Shumway, S.E., Tester, P.A., 1997. Harmful Algal Blooms in Coastal Waters: Options for Prevention, Control and Mitigation. NOAA Coastal Ocean Program Decision Analysis Series No. 10 46. NOAA Coastal Office, Silver Spring, MD, USA, pp. 201–261. https://repository.library.noaa.gov/view/noaa/1513.

Carter, J.G., Cavan, G., Connelly, A., Guy, S., Handley, J., Kazmierczak, A., 2015. Climate change and the city: building capacity for urban adaptation. Prog. Plann. 95, 1–66. https://doi.org/10.1016/j.progress.2013.08.001.

Chen, J., Brissette, F.P., Chaumont, D., Braun, M., 2013. Finding appropriate bias correction methods in downscaling precipitation for hydrologic impact studies over North America. Water Resour. Res. 49, 4187–4205. https://doi.org/10.1002/wrcr.20331.

Chiew, F.H.S., McMahon, T.A., 2002. Modelling the impacts of climate change on Australian streamflow. Hydrol. Process. 16 (6), 1235–1245. https://doi.org/10.1002/hyp.1059.

Cuo, L., Zhang, Y., Gao, Y., Hao, Z., Cairang, L., 2013. The impacts of climate change and land cover/use transition on the hydrology in the upper Yellow River Basin. China. J. Hydrol. 502, 37–52. https://doi.org/10.1016/j.jhydrol.2013.08.003.

Diem, J.E., Hill, T.C., Milligan, R.A., 2018. Diverse multi-decadal changes in streamflow within a rapidly urbanizing region. J. Hydrol. 556, 61–71. https://doi.org/10.1016/j.jhydrol.2017.10.026.

Environmental Systems Research Institute (ESRI), 2018. ArcGIS Desktop: Release 10.6. Redlands, CA, USA. https://www.esri.com/en-us/arcgis/products/arcgis-desktop/overview.

Falconer, R.H., Cobby, D., Smyth, P., Astle, G., Dent, J., Golding, B., 2009. Pluvial flooding: new approaches in flood warning, mapping and risk management. J. Flood Risk Manage. 2 (3), 198–208. https://doi.org/10.1111/j.1753-318X.2009.01034.x.

Franczyk, J., Chang, H., 2009. The effects of climate change and urbanization on the runoff of the Rock Creek Basin in the Portland metropolitan area, OR, USA. Hydrol. Processes. 23 (6), 805–815. https://doi.org/10.1002/hyp.7176.

Fry, J.A., Xian, G., Jin, S., Dewitz, J.A., Homer, C.G., Yang, L., Barnes, C.A., Herold, N.D., Wickham, J.D., 2011. Completion of the 2006 national land cover database for the conterminous United States. Photogramm. Eng. Remote. Sens. 77 (9), 858–864. https://cfpub.epa.gov/si/si_public_record_report.cfm?Lab=NERL&dirEntryId=237844.

Fukunaga, D.C., Cecílio, R.A., Zanetti, S.S., Oliveira, L.T., Caiado, M.A.C., 2015. Application of the SWAT hydrologic model to a tropical watershed at Brazil. Catena 125, 206–213. https://doi.org/10.1016/j.catena.2014.10.032.

Ghani, A.A., Ali, R., Zakaria, N.A., Hasan, Z.A., Chang, C.K., Ahamad, M.S.S., 2010. A temporal change study of the Muda River system over 22 years. Int. J. River Basin Manag. 8, 25–37. https://doi.org/10.1080/15715121003715040.

Hallegatte, S., Green, C., Nicholls, R.J., Corfee-Morlot, J., 2013. Future flood losses in major coastal cities. Nat. Clim. Chang. 3 (9), 802–806. https://doi.org/10.1038/NCLIMATE1979.

Hanasaki, N., Kanae, S., Oki, T., Masuda, K., Motoya, K., Shirakawa, N., Shen, Y., Tanaka, K., 2008a. An integrated model for the assessment of global water resources–part 1: model description and input meteorological forcing. Hydrol. Earth Syst. Sci. 12 (4), 1007–1025. https://www.hydrol-earth-syst-sci.net/12/1007/2008/.

Hanasaki, N., Kanae, S., Oki, T., Masuda, K., Motoya, K., Shirakawa, N., Shen, Y., Tanaka, K., 2008b. An integrated model for the assessment of global water resources–part 2: applications and assessments. Hydrol. Earth Syst. Sci. 12 (4), 1027–1037. https://www.hydrol-earth-syst-sci.net/12/1027/2008/.

Hasan, E., Tarhule, A., Kirstetter, P.E., Clark, R., Hong, Y., 2018. Runoff sensitivity to climate change in the Nile River Basin. J. Hydrol. 561, 312–321. https://doi.org/10.1016/j.jhydrol.2018.04.004.

Homer, C., Dewitz, J., Yang, L., Jin, S., Danielson, P., Xian, G., Coulston, J., Herold, N., Wickham, J., Megown, K., 2015. Completion of the 2011 national land cover database for the conterminous United States—representing a decade of land cover change

information. Photogramm. Eng. Remote. Sens. 81 (5), 345–354. https://pubs.er.usgs.gov/publication/70146301.
Hovenga, P.A., Wang, D., Medeiros, S.C., Hagen, S.C., Alizad, K., 2016. The response of runoff and sediment loading in the Apalachicola River, Florida to climate and land use land cover change. Earth's Futur. 4, 124–142. https://doi.org/10.1002/2015EF000348.
Hu, S., Shrestha, P., 2020. Examine the impact of land use and land cover changes on peak discharges of a watershed in the midwestern United States using the HEC-HMS model. Pap. Appl. Geogr. 6, 101–118. https://doi.org/10.1080/23754931.2020.1732447.
Hughes, J.D., White, J.T, 2016. Hydrologic conditions in urban Miami-Dade County, Florida, and the effect ofgroundwater pumpage and increased sea level on canal leakage and regional groundwater flow (ver. 1.2, July 2016). U.S. Geological Survey Scientific Investigations Report, pp. 2014–5162 https://doi.org/10.3133/sir20145162.
Intergovernmental Panel on Climate Change (IPCC), 2014a. Climate Change 2014: Impacts, Adaptation, and Vulnerability. Part A: Global and Sectoral Aspects. Contribution of Working Group II to the Fifth Assessment Report of the Intergovernmental Panel on Climate Change [C.B. Field, V.R. Barros, D.J. Dokken, K.J. Mach, M.D. Mastrandrea, T.E. Bilir, M. Chatterjee, K.L. Ebi, Y.O. Estrada, R.C. Genova, B. Girma, E.S. Kissel, A.N. Levy, S. MacCracken, P.R. Mastrandrea, and L.L. White (eds.)]. Cambridge University Press, Cambridge, UK and New York, NY, USA. https://www.ipcc.ch/site/assets/uploads/2018/02/WGIIAR5-PartA_FINAL.pdf.
Intergovernmental Panel on Climate Change (IPCC), 2014b. Climate Change 2014: Synthesis Report. Contribution of Working Groups I, II and III to the Fifth Assessment Report of the Intergovernmental Panel on Climate Change [Core Writing Team, R.K. Pachauri and L.A. Meyer (eds.)]. IPCC, Geneva, Switzerland. https://epic.awi.de/id/eprint/37530/.
Jacobson, C.R., 2011. Identification and quantification of the hydrological impacts of imperviousness in urban catchments: a review. J. Environ. Manag. 92 (6), 1438–1448. https://doi.org/10.1016/j.jenvman.2011.01.018.
Julien, P.Y., Ghani, A.A., Zakaria, N.A., Abdullah, R., Chang, C.K., 2010. Case study: flood mitigation of the Muda River, Malaysia. J. Hydraul. Eng. 136, 251–261. https://doi.org/10.1061/(asce)hy.1943-7900.0000163.
Kottek, M., Grieser, J., Beck, C., Rudolf, B., Rubel, F., 2006. World map of the Köppen-Geiger climate classification updated. Meteorol. Z. 15 (3), 259–263. https://doi.org/10.1127/0941-2948/2006/0130.
Langousis, A., Mamalakis, A., Deidda, R., Marrocu, M., 2016. Assessing the relative effectiveness of statistical downscaling and distribution mapping in reproducing rainfall statistics based on climate model results. Water Resour. Res. 52 (1), 471–494. https://doi.org/10.1002/2015WR017556.
Lapointe, B.E., Herren, L.W., Bedford, B.J., 2012. Effects of hurricanes, land use, and water management on nutrient and microbial pollution: St. Lucie Estuary. Southeast Florida. J. Coast. Res. 28 (6), 1345–1361. https://doi.org/10.2112/JCOASTRES-D-12-00070.1.
Li, C., Liu, M., Hu, Y., Shi, T., Qu, X., Walter, M.T., 2018. Effects of urbanization on direct runoff characteristics in urban functional zones. Sci. Total Environ. 643, 301–311. https://doi.org/10.1016/j.scitotenv.2018.06.211.
Liang, X., Lettenmaier, D.P., Wood, E.F., 1994. A simple hydrologically based model of land surface water and energy fluxes for general circulation models. J. Geophys. Res. Atmos. 99 (D7), 14415–14428. https://doi.org/10.1029/94JD00483.
Liu, Q., Qin, Y., Zhang, Y., Li, Z., 2015. A coupled 1D–2D hydrodynamic model for flood simulation in flood detention basin. Nat. Hazards. 75, 1303–1325. https://doi.org/10.1007/s11069-014-1373-3.
Lu, Z., Fu, Z., Hua, L., Yuan, N., Chen, L., 2018. Evaluation of ENSO simulations in CMIP5 models: a new perspective based on percolation phase transition in complex networks. Sci. Rep. 8 (1), 14912. https://doi.org/10.1038/s41598-018-33340-y.
Maidment, D., Morehouse, S., 2002. ArcHydro: GIS for Water Resources. ESRI Press, Redlands, CA, USA.
Mateus, C., Tullos, D.D., Surfleet, C.G., 2015. Hydrologic sensitivity to climate and land use changes in the Santiam River Basin, Oregon. J. Am. Water Resour. Assoc. 51 (2), 400–420. https://doi.org/10.1111/jawr.12256.
Miller, J.D., Kim, H., Kjeldsen, T.R., Packman, J., Grebby, S., Dearden, R., 2014. Assessing the impact of urbanization on storm runoff in a peri-urban catchment using historical change in impervious cover. J. Hydrol. 515, 59–70. https://doi.org/10.1016/j.jhydrol.2014.04.011.
Moriasi, D.N., Arnold, J.G., Van Liew, M.W., Bingner, R.L., Harmel, R.D., Veith, T.L., 2007. Model evaluation guidelines for systematic quantification of accuracy in watershed simulations. Trans. ASABE 50 (3), 885–900. https://pubag.nal.usda.gov/catalog/9298.
Morris, F. W., 1986. Bathymetry of the St. Lucie estuary. Technical publication 86-4. Water resources division, resource planning management, South Florida Water Management District, West Palm Beach, FL, USA.
Nakicenovic, N., Alcamo, J., Davis, G., Vries, B.d., Fenhann, J., Gaffin, S., Gregory, K., Grübler, A., Jung, T. Y., Kram, T., Rovere, E. L. L., Michaelis, L., Mori, S., Morita, T., Pepper, W., Pitcher, H., Price, L., Riahi, K., Roehrl, A., Rogner, H.-H., Sankovski, A., Schlesinger, M., Shukla, P., Smith, S., Swart, R., Rooijen, S. V., Victor, N., Dadi, Z., 2000. Special report on emissions scenarios, A special report of working group III of the intergovernmental panel on climate change. Cambridge University Press, Cambridge, UK. http://pure.iiasa.ac.at/id/eprint/6101/.
Nash, J.E., Sutcliffe, J.V., 1970. River flow forecasting through conceptual models part I—a discussion of principles. J. Hydrol. 10 (3), 282–290. https://doi.org/10.1016/0022-1694(70)90255-6.
National Oceanic and Atmospheric Administration (NOAA), 2017a. Tides & Currents. Accessed on April 15, 2017 from https://tidesandcurrents.noaa.gov/.
National Oceanic and Atmospheric Administration (NOAA), 2017b. National Climatic Data Center. Accessed on April 23, 2017 from https://www.ncdc.noaa.gov/.
National Oceanic and Atmospheric Administration (NOAA), 2021. 1981–2010 Normals. Accessed on February 03, 2021 from https://www.ncdc.noaa.gov/.
Natural Resources Conservation Service (NRCS), 2009. National Engineering Handbook, title 210-VI, part 630, chapter 7. United States Department of Agriculture, Washington, D.C., USA. Accessed on April 08, 2017 from https://www.nrcs.usda.gov/wps/portal/nrcs/detailfull/national/water/?&cid=stelprdb1043063.
Natural Resources Conservation Service (NRCS), 2015. Soil Survey Geographic (SSURGO) database for Florida – June 2012. United States Department of Agriculture, Washington, D.C., USA. Accessed on January 05, 2015 from http://www.fgdl.org/metadataexplorer/explorer.jsp.
Neitsch, S.L., Arnold, J.G., Kiniry, J.R., Williams, J.R., 2005. Soil and Water Assessment Tool Theoretical Documentation Version 2005. Soil and Water Research Laboratory. ARS, Temple, TX, USA.
Obeysekera, J., Park, J., Irizarry-Ortiz, M., Trimble, P., Barnes, J., VanArman, J., Said, W., Gadzinski, E., 2011. Past and projected trends in climate and sea level for south Florida. South Florida Water Management District interdepartmental climate change group, hydrologic and environmental systems modeling technical report. July 5, 2011, West Palm Beach, FL, USA. https://www.sfwmd.gov/document/past-and-projected-trends-climate-and-sea-level-south-florida.
Obeysekera, J., Barnes, J., Nungesser, M., 2015. Climate sensitivity runs and regional hydrologic modeling for predicting the response of the greater Florida Everglades ecosystem to climate change. Environ. Manag. 55 (4), 749–762. https://doi.org/10.1007/s00267-014-0315-x.
Olang, L.O., Fürst, J., 2011. Effects of land cover change on flood peak discharges and runoff volumes: model estimates for the Nyando River Basin. Kenya. Hydrol. Processes. 25 (1), 80–89. https://doi.org/10.1002/hyp.7821.
Olivera, F., DeFee, B.B., 2007. Urbanization and its effect on runoff in the Whiteoak Bayou Watershed, Texas. J. Am. Water Resour. Assoc. 43 (1), 170–182. https://doi.org/10.1111/j.1752-1688.2007.00014.x.
Oo, H.T., Zin, W.W., Thin Kyi, C.C., 2020. Analysis of streamflow response to changing climate conditions using SWAT model. Civ. Eng. J. 6, 194–209. https://doi.org/10.28991/cej-2020-03091464.
ORNL DAAC, 2017. Spatial Data Access Tool (SDAT). ORNL DAAC, Oak Ridge, TN, USA. Accessed on September 12, 2017 from https://doi.org/10.3334/ORNLDAAC/1388.
Öztürk, M., Copty, N.K., Saysel, A.K., 2013. Modeling the impact of land use change on the hydrology of a rural watershed. J. Hydrol. 497, 97–109. https://doi.org/10.1016/j.jhydrol.2013.05.022.
Pathak, C.S., 2001. Frequency analysis of daily rainfall maxima for central and south Florida. Technical Publication EMA-390. South Florida Water Management District, West Palm Beach, FL, USA.
Pumo, D., Arnone, E., Francipane, A., Caracciolo, D., Noto, L.V., 2017. Potential implications of climate change and urbanization on watershed hydrology. J. Hydrol. 554, 80–99. https://doi.org/10.1016/j.jhydrol.2017.09.002.
Rai, P.K., Chahar, B.R., Dhanya, C.T., 2017. GIS-based SWMM model for simulating the catchment response to flood events. Hydrol. Res. 48, 384–394. https://doi.org/10.2166/nh.2016.260.
Rawls, W.J., Brakensiek, D.L., Miller, N., 1983. Green-Ampt infiltration parameters from soils data. J. Hydraul. Eng. 109 (1), 62–70. https://doi.org/10.1061/(ASCE)0733-9429(1983)109:1(62).
Rosenzweig, B.R., McPhillips, L., Chang, H., Cheng, C., Welty, C., Matsler, M., Iwaniec, D., Davidson, C.I., 2018. Pluvial flood risk and opportunities for resilience. Wiley Interdiscip. Rev. Water. 5 (6), 1–18. https://doi.org/10.1002/wat2.1302.
Rossman, L. A., 2015. Storm Water Management Model user's manual, version 5.1, report EPA-600/R-14/413b. National risk management research laboratory, office of research and development, U.S. Environmental Protection Agency. Cincinnati, OH, USA. http://nepis.epa.gov/Exe/ZyPDF.cgi?Dockey=P100N3J6.TXT.
Rossman, L.A., Huber, W., 2016. Storm water management model reference manual volume I–hydrology (revised), report EPA/600/R-15/162A. National Risk Management Research Laboratory, Office of Research and Development. Cincinnati, OH, USA, U.S. Environmental Protection Agency http://nepis.epa.gov/Exe/ZyPDF.cgi?Dockey=P100NYRA.txt.
Rubel, F., Brugger, K., Haslinger, K., Auer, I., 2017. The climate of the European Alps: shift of very high resolution Köppen-Geiger climate zones 1800–2100. Meteorol. Zeitschrift 26, 115–125. https://doi.org/10.1127/metz/2016/0816.
Schmidt, N., Lipp, E.K., Rose, J.B., Luther, M.E., 2001. ENSO influences on seasonal rainfall and river discharge in Florida. J. Clim. 14 (4), 615–628. https://doi.org/10.1175/1520-0442(2001)014<0615:EIOSRA>2.0.CO;2.
South Florida Water Management District (SFWMD), 2017. DBHYDRO (environmental data). Accessed on January 10, 2017 from https://www.sfwmd.gov/science-data/dbhydro.
Southeast Florida Regional Climate Change Compact (SFRCCC) Sea Level Rise Work Group, 2015. Unified Sea Level Rise Projection for Southeast Florida. A document prepared for the Southeast Florida Regional Climate Change Compact Steering Committee. 1–35.
Sunde, M.G., He, H.S., Hubbart, J.A., Urban, M.A., 2018. An integrated modeling approach for estimating hydrologic responses to future urbanization and climate changes in a mixed-use midwestern watershed. J. Environ. Manag. 220, 149–162. https://doi.org/10.1016/j.jenvman.2018.05.025.
Teutschbein, C., Seibert, J., 2012. Bias correction of regional climate model simulations for hydrological climate-change impact studies: review and evaluation of different methods. J. Hydrol. 456–457, 12–29. https://doi.org/10.1016/j.jhydrol.2012.05.052.
The MathWorks, Inc., 2018. MATLAB. Version 2018b. Natick, MA, USA https://www.mathworks.com/products/new_products/release2018b.html.
Tukey, J.W., 1977. Exploratory Data Analysis. Addison-Wesley, Reading, Massachusetts https://doi.org/10.1002/bimj.4710230408.
Ul Islam, S., Curry, C.L., Déry, S.J., Zwiers, F.W., 2019. Quantifying projected changes in runoff variability and flow regimes of the Fraser River Basin. British Columbia. Hydrol. Earth Syst. Sci. 23, 811–828. https://doi.org/10.5194/hess-23-811-2019.

United States Army Corps of Engineers (USACE), 2000. Hydrologic modeling system HEC-HMS users manual, version 2.0. Hydrologic Engineering Center, US Army Corps of Engineers, Davis, CA, USA.

United States Environmental Protection Agency (U.S. EPA), 2010. ICLUS tools and datasets (Version 1.3.2). U.S. Environmental Protection Agency, Washington, D.C., USA. EPA/600/R-09/143F. Accessed on October 30, 2017 from https://cfpub.epa.gov/ncea/global/recordisplay.cfm?deid=257306.

United States Geological Survey (USGS), 2016a. The national map. Accessed on February 03, 2016 from https://viewer.nationalmap.gov/basic/.

United States Geological Survey (USGS), 2016b. National elevation dataset (NED). Accessed on February 16, 2016 from https://lta.cr.usgs.gov/NED.

United States Geological Survey (USGS), 2016c. Evapotranspiration information and data. Accessed on February 20, 2016 from https://fl.water.usgs.gov/et/.

United States Geological Survey (USGS), 2017a. Surface-water data for the nation. Accessed on January 08, 2017 from https://waterdata.usgs.gov/nwis/sw.

United States Geological Survey (USGS), 2017b. Groundwater data for the nation. Accessed on January 08, 2017 from https://waterdata.usgs.gov/nwis/gw.

Urban Drainage and Flood Control District, 2016. Urban storm drainage criteria manual: volume 1 management, hydrology, and hydraulics. Urban Drainage and Flood Control District. Denver, CO, USA. https://udfcd.org/volume-one.

Van Vuuren, D.P., Carter, T.R., 2014. Climate and socio-economic scenarios for climate change research and assessment: reconciling the new with the old. Clim. Chang. 122 (3), 415–429. https://doi.org/10.1007/s10584-013-0974-2.

Wagesho, N., Jain, M.K., Goel, N.K., 2012. Effect of climate change on runoff generation: Application to rift valley lakes basin of Ethiopia. J. Hydraul. Eng. 18 (8), 1048–1063. https://doi.org/10.1061/(ASCE)HE.1943-5584.0000647.

Wang, H., Stephenson, S.R., 2018. Quantifying the impacts of climate change and land use/cover change on runoff in the lower Connecticut River Basin. Hydrol. Process. 32 (9), 1301–1312. https://doi.org/10.1002/hyp.11509.

Wang, G., Zhang, J., He, R., Liu, C., Ma, T., Bao, Z., Liu, Y., 2017. Runoff sensitivity to climate change for hydro-climatically different catchments in China. Stoch. Environ. Res. Risk Assess. 31, 1011–1021. https://doi.org/10.1007/s00477-016-1218-6.

Wang, J., Hu, C., Ma, B., Mu, X., 2020. Rapid urbanization impact on the hydrological processes in Zhengzhou. China. Water (Switzerland) 12. https://doi.org/10.3390/W1207187.

Zainalfikry, M.K., Ab Ghani, A., Zakaria, N.A., Chan, N.W., 2020. HEC-RAS one-dimensional hydrodynamic modelling for recent major flood events in Pahang River. Lect. Notes Civ. Eng. 53, 1099–1115. https://doi.org/10.1007/978-3-030-32816-0_83.

Zhang, X.C., 2013. Verifying a temporal disaggregation method for generating daily precipitation of potentially non-stationary climate change for site-specific impact assessment. Int. J. Climatol. 33 (2), 326–342. https://doi.org/10.1002/joc.3425.

Zhang, Y., Wang, G., 2007. Impact of Climate Change on Hydrology and Water Resources. China Science Press, Beijing, China.

Zhao, S., Deng, Y., Black, R.X., 2017. Observed and simulated spring and summer dryness in the United States: the impact of the Pacific Sea surface temperature and beyond. J. Geophys. Res. Atmos. 122 (23), 12713–12731. https://doi.org/10.1002/2017JD027279.

Zheng, H., Chiew, F.H., Charles, S., Podger, G., 2018. Future climate and runoff projections across South Asia from CMIP5 global climate models and hydrological modelling. J. Hydrol.: Reg. Stud. 18, 92–109. https://doi.org/10.1016/j.ejrh.2018.06.004.